HHS Public Access

Author manuscript

Cancer Cell. Author manuscript; available in PMC 2018 September 11.

Published in final edited form as:

Cancer Cell. 2017 September 11; 32(3): 377–391.e9. doi:10.1016/j.ccell.2017.08.004.

Enhancing CD8+ T cell fatty acid catabolism within a metabolically challenging tumor microenvironment increases the efficacy of melanoma immunotherapy

Ying Zhang[1,2,9], **Raj Kurupati**[2], **Ling Liu**[3], **Xiang Yang Zhou**[2], **Gao Zhang**[2], **Abeer Hudaihed**[4], **Flavia Filisio**[4], **Wynetta Giles-Davis**[2], **Xiaowei Xu**[5], **Giorgos C. Karakousis**[6], **Lynn M. Schuchter**[7], **Wei Xu**[7], **Ravi Amaravadi**[7], **Min Xiao**[2], **Norah Sadek**[2], **Clemens Krepler**[2], **Meenhard Herlyn**[2], **Gordon J Freeman**[8], **Joshua D Rabinowitz**[3], and **Hildegund CJ Ertl**[2,10,*]

[1]Gene Therapy & Vaccines Program, University of Pennsylvania (U of PA), Philadelphia, PA 19104, USA

[2]The Wistar Institute, Philadelphia, PA 19104, USA

[3]Lewis-Sigler Institute for Integrative Genomics & Department of Chemistry, Princeton University, Princeton, NJ 08540, USA

[4]Biology Program, Temple University, Philadelphia, PA 19122, USA

[5]Department of Pathology and Laboratory Medicine, U of PA, Philadelphia, PA 19104, USA

[6]Department of Surgery, Hospital of U of PA, Philadelphia, PA 19104, USA

[7]Department of Medicine, U of PA, Philadelphia, PA 19104, USA

[8]Department of Medical Oncology, Dana-Farber Cancer Institute, Boston, MA 02115, USA

Summary

How tumor-infiltrating T lymphocytes (TILs) adapt to the metabolic constrains within the tumor microenvironment (TME) and to what degree this affects their ability to combat tumor progression remain poorly understood. Using mouse melanoma models, we report that $CD8^+$ TILs enhance PPAR-α signaling and catabolism of fatty acids (FAs) when simultaneously subjected to hypoglycemia and hypoxia. This metabolic switch partially preserves $CD8^+$ TILs' effector functions although co-inhibitor expression increases during tumor progression regardless of their antigen specificity. Further promoting FA catabolism improves the $CD8^+$ TIL's ability to slow tumor progression. PD-1 blockade delays tumor growth without changing TIL metabolism or functions. It synergizes with metabolic reprogramming of T cells to achieve superior antitumor efficacy and even complete cures.

*Correspondence: ertl@wistar.org.

[9]Current Address: Program in Cellular and Molecular Medicine, Boston Children's Hospital, Boston, MA 02115, USA

[10]Lead Contact

AUTHOR CONTRIBUTIONS

YZ - design, experiments, data analyses, writing; RK - experiments; LL - metabolomics studies; XYZ- cloning design; AH, FF-assisted YZ; WG-D - cell culture; XWX, GK, LS, WX and RA - human samples collection; GF - α-PD-1 Ab; JR - metabolomics studies; GZ, MX, NS, CK, MH - PDX model; HE - design, data analyses, writing.

Keywords

Melanoma; tumor microenvironment; $CD8^+$ T cells; TILs; co-inhibitors; hypoxia; HIF-1α; hypoglycemia; fatty acid catabolism; fenofibrate

INTRODUCTION

Despite recent progress in cancer immunotherapy, cures remain rare. Transfer of *ex vivo* expanded TILs may affect tumor regression, but vaccines that induce such T cells have largely been ineffective (Dalgleish, 2011). This has been linked to exhaustion of tumor antigen (TA)-specific $CD8^+$ TILs characterized by enhanced expression of co-inhibitors and loss of functions following chronic antigen stimulation (Mueller and Ahmed, 2009). Treatment with immune checkpoint inhibitors can improve TIL functions and is yielding promising results in patients (Zou et al., 2016).

Upon activation T cells enhance glycolysis to support energy and biomass production. Tumor cells also use glycolysis (Hamanaka and Chandel, 2012), which may lead to glucose (Glc) depletion within the TME. T cells with limited access to Glc switch to oxidative phosphorylation (OXPHOS). Although many nutrients fuel OXPHOS, it requires oxygen (O_2), which due to insufficient blood supply can become limiting within tumors. TILs therefore face dual metabolic jeopardy, which may impair the efficacy of T cell-mediated cancer therapy.

How $CD8^+$ TILs metabolically adapt to the nutrient and O_2-limited TME and how these adjustments affect their tumor-killing functions are not well understood. In this study, we investigated the effects of metabolic challenges within the TME on $CD8^+$ T cells and designed interventions that may allow for better preservation of $CD8^+$ TIL functions.

RESULTS

$CD8^+$ T cells become functionally impaired within the TME regardless of their antigen specificity

To test if the fate of $CD8^+$ TILs depends on continued antigen stimulation, we used two vaccines in a transplantable mouse melanoma model. AdC68-gDMelapoly (Figure 1A) is an adenovirus (Ad)-based vaccine that elicits melanoma-associated antigen (MAA)-specific $CD8^+$ T cell responses mainly to the Trp-$1_{455\text{-}463}$ epitope (Zhang and Ertl, 2014). AdC68-gDE7 stimulates $CD8^+$ T cells to human papilloma virus (HPV) E7 (Lasaro et al., 2008). We vaccinated mice bearing 3-day $B16Braf_{V600E}$ tumors and normal mice with AdC68-gDMelapoly mixed with AdC68-gDE7. Vaccination delays tumor progression (Figure 1B). Both MAA- and E7-specific $CD8^+$ T cells accumulate within tumors, where they contract more rapidly than in the periphery (Figure 1C). Numbers of MAA-specific $CD8^+$ TILs decline by >90% between day 10 and 30 after vaccination while E7-specific $CD8^+$ TILs decline by ~80%. This prominent reduction in MAA-specific $CD8^+$ TIL numbers occurs although they proliferate before entering tumors or within the TME (Figure 1D). Nevertheless, proliferation decreases over time despite continued presence of their antigens (not shown). MAA- and E7-specific $CD8^+$ T cells from day 14 and, to a more pronounced

extent, day 30 tumors increase expression of PD-1 and LAG-3 (Figure 1E). During tumor progression, frequencies of $CD8^+$ T cells producing the effector molecules granzyme B (GrmB), perforin and interferon (IFN)-γ decline faster in tumors than in spleens and by day 30 after challenge $CD8^+$ TILs lose polyfunctionality (Figure 1F). These data suggest that TILs regardless of their antigen specificity differentiate towards functional exhaustion during tumor progression, contesting the notion that sustained antigen stimulation is required to drive TIL exhaustion (Bucks et al., 2009). Ad vectors persist at low levels and thus maintain high frequencies of functional effector $CD8^+$ T cells (Tatsis et al., 2007). Accordingly, most vaccine-induced MAA- (Figure 1G) and E7- (not shown) specific $CD8^+$ T cells remain $CD44^{hi}CD62L^{lo}CD127^{lo}KLRG1^{hi}$ during tumor progression. Levels of T-bet and Eomes decrease in specific T cells from spleens and tumors over time, presumably reflecting differentiation driven by reduced antigenic load in spleens and progression towards exhaustion in tumors (Zhu et al., 2010).

To determine whether exhaustion of TILs occurs independent of vaccination, we transfused mice bearing 5-day $B16_{OVA}$ tumors with OT-1 splenocytes, which carry a transgenic T cell receptor to SIINFEKL, the immunodominant epitope of ovalbumin (OVA). Few OT-1 T cells infiltrate day 14 tumors; more are detected in day 30 tumors. OT-1 TILs from day 30 tumors compared to those from spleens or day 14 tumors increase PD-1 and LAG-3 and decrease CD62L (Figure S1A) and IFN-γ production (Figure S1B), suggesting that in both models TILs become exhausted. This process may not be solely driven by chronic antigen stimulation (Bucks et al., 2009) as shown with vaccine-induced $CD8^+$ TILs.

Metabolism dictates cellular fate and could affect $CD8^+$ TILs independent of their antigen specificity. During tumor progression MAA- and E7-specific $CD8^+$ TILs lose mitochondrial membrane potential (MMP) and increase levels of mitochondrial reactive oxygen species (MROS) (Figure 2A). $MMP^{lo}MROS^{hi}$ MAA- and to a lesser extent E7-specific $CD8^+$ TILs become prevalent in day 30-tumors (Figure 2B), while corresponding $CD8^+$ T cells from spleens remain largely $MMP^{hi}MROS^{lo}$. We controlled the specificities of mitochondrial stains (Figure 2C) and confirmed that changes in MMP and MROS levels are not due to cell size differences (Figure 2D). Electron microscopy shows that mitochondria within $CD44^+CD8^+$ TILs from advanced tumors lose the typical rod-like structure as described (Siska et al., 2017). They display poorly defined membranes and cristae compared to those in splenic T cells (Figure 2E), confirming that $CD8^+$ TILs experience mitochondrial stress within growing tumors.

Hypoxia through HIF-1α increases LAG-3 expression and impairs T cell functions

MAA- and E7-specific $CD8^+$ TILs are subjected to hypoxia during tumor progression as shown by enhanced expressions of HIF-1α, the main transcriptional regulator in the cells' response to hypoxia, and its downstream target Glut1, which facilitates Glc uptake (Figure 3A).

To determine how hypoxia affects $CD8^+$ T cells, we stimulated them *in vitro* for 4 days under normoxia (21% O_2) or for the last 16 hr under hypoxia (1% O_2, Figure S2A). Hypoxia reduces blast formation (Figure S2B) and increases expression of HIF-1α and Glut1 (Figure S2C). The O_2 consumption rate (OCR), a measure of OXPHOS, decreases under hypoxia

while the extracellular acidification rate (ECAR), a measure of glycolysis, increases (Figure S2D). The T cells' MMP decreases and MROS increases, leading to a rise in $MMP^{lo}MROS^{hi}$ $CD8^+$ T cells (Figure S2E) as in vaccine-induced TILs from late-stage tumors. Hypoxia reduces PD-1 but augments LAG-3 (Figure S2F), suggesting both are modulated upon HIF-1α activation. $CD8^+$ T cells cultured under hypoxia decrease T-bet (Figure S2F), production of effector molecules and polyfunctionality (Figure S2G). A previously described protocol (Doedens et al., 2013), in which $CD8^+$ T cells after initial activation are maintained at a more resting stage in IL-2 and exposed to hypoxia (Figure S2H), has no effect on blast formation (Figure S2I) or PD-1, although LAG-3 increases and T-bet decreases (Figure S2J). GrmB production increases while production of other effector molecules and polyfunctionality decline (Figure S2K). As vaccine-induced MAA-specific $CD8^+$ T cells are unlikely to rest before infiltrating the TME's hypoxic areas, we used the protocol of continuous $CD8^+$ T cell activation for subsequent experiments.

HIF-1α positively correlates with expression of LAG-3 on TILs or $CD8^+$ T cells subjected to hypoxia (Figure S3A). To determine whether HIF-1α directly promotes LAG-3 expression, we first knocked down (KD) HIF-1α using three lentivectors that express different HIF-1α-silencing short hairpin RNAs (shRNAs) or a scrambled shRNA. Each lentivector that reduces HIF-1α in activated $CD8^+$ T cells also reduces Glut1 and LAG-3, increases GrmB, and decreases perforin production (Fig S3B–D), suggesting the results are not due to off-target effects. We used HIF-1α shRNA lentivector E1676 for *in vitro* studies and for the vaccine model. E1676 transduces ~ 34% of activated $CD8^+$ T cells (Figure S3E) and achieves 20% and 60% reduction of HIF-1α transcripts under normoxia or hypoxia, respectively (Figure S3F). Under hypoxia HIF-1α KD decreases LAG-3 but not PD-1 on $CD8^+$ T cells (Figure S3G), and improves production of GrmB and IFN-γ (Figure S3H).

To study how HIF-1α signaling affects $CD8^+$ TILs, we activated $CD8^+$ T cells *in vitro* and, after lentivector transduction, transferred them into tumor-bearing, AdC68-gDMelapoly-vaccinated mice (Figure 3B). We analyzed the transferred T cells ~3 weeks later from similar sized tumors (Figure S3I). HIF-1α KD, which remains stable after cell transfer (Figure 3C), reduces the MAA-specific $CD8^+$ TILs' expression of LAG-3 without affecting PD-1 (Figure 3D), and improves their effector functions including polyfunctionality (Figure 3E).

To further study the effect of HIF-1α on $CD8^+$ TILs, we knocked down HIF-1α in activated OT-1 $CD8^+$ T cells with a mixture of the three HIF-1α shRNA lentivectors. Approximately 75% of cells are transduced (Figure S3J). They show 50% reduction in HIF-1α transcripts (Figure S3K) and protein expression, combined with modest decreases in surface Glut1 (Figure S3L). HIF-1α KD reduces levels of transcripts encoding enzymes of glycolysis and with a delay increases transcripts for factors involved in the tricarboxylic acid (TCA) cycle and FA catabolism (Figure S3M).

Transduced $Thy1.1^+$ OT-1 cells were transferred into mice bearing 5-day $B16_{OVA}$ tumors (Figure 3F). Tumor progression is delayed in mice transferred with HIF-1α shRNA-treated OT-1 $CD8^+$ T cells (Figure 3G). TILs from day 20 tumors show comparable differentiation between the two groups (Figure S3N) and HIF-1α KD remains stable (Figure S3O). HIF-1α

KD reduces LAG-3 without changing PD-1 on TILs. It increases T-bet (Figure 3H) and effector functions (Figure 3I). Levels of transcripts indicative of glycolysis decrease; those for the TCA cycle increase (Figure 3J). Accordingly, TILs with HIF-1α KD decrease Glut1 but enhance PPAR-α, a key transcription factor that promotes FA catabolism and uptake of FAs (Figure 3K). These data show that HIF-1α KD in TA-specific TILs reduces glycolysis and promotes OXPHOS. They further suggest that HIF-1α-driven increases in glycolysis might be counterproductive to T cell functions within an O_2 and Glc -depleted TME.

Activated $CD8^+$ T cells lacking both Glc and O_2 enhance FA catabolism

Not only O_2 but also Glc declines within the TME during tumor progression (Figure 4A). We studied the collective effects of hypoglycemia and hypoxia on $CD8^+$ T cells by stimulating them *in vitro* in Glc-medium with the glycolysis inhibitor 2-deoxy-D-glucose (2-DG) or replacing Glc with galactose (Gal). Cells were cultured under normoxia or short-term hypoxia. Either condition decreases ECAR and augments the OCR/ECAR ratio (Figure S4A), suggesting increased energy production through OXPHOS. Cells cultured with 2-DG or Gal rather than Glc increase PD-1, indicating that OXPHOS is linked to high PD-1 expression on activated $CD8^+$ T cells (Figure S4B). Compared to cells cultured with Glc, those with limited Glc decrease T-bet (Figure S4C) and lose functions and polyfunctions (Figure S4D). Polyfunctions of $CD8^+$ T cells with limited Glc supply are better preserved if cells are also subjected to hypoxia, suggesting that cells may more readily cope with hypoglycemia with increased HIF-1α signaling.

To study the metabolic pathways used by Glc- and O_2-starved $CD8^+$ T cells, we measured transcripts for factors that participate in nutrient consumption and energy production (Figure S4E, S4F, 4B). Upon short-term hypoxia $CD8^+$ T cells stimulated under hypoglycemia rather than in Glc-medium decrease transcripts for factors of glycolysis, TCA cycle, ROS detoxification and electron transport chain (ETC). They show increased transcripts of PPAR-α and downstream molecules involved in FA uptake, triglyceride (TG) turnover, peroxisomal and mitochondrial FA catabolism. This pattern is mirrored by MAA- and E7-specific $CD8^+$ TILs from day 30 vs. 14 tumors, indicating that metabolically stressed $CD8^+$ TILs increasingly rely on FA catabolism. Changes in transcripts during tumor progression are not driven by TIL differentiation towards a more resting stage, as they are distinct from those in vaccine-induced splenic $CD8^+$ T cells tested at 90 vs. 14 days after vaccination.

To directly measure effects of Glc and O_2 deprivation on $CD8^+$ T cell metabolism, we analyzed the intensity of metabolites by lipid chromatography-mass spectrometry (LC-MS). Metabolites of FA catabolism, i.e., acetylcarnitine, palmitoylcarnitine, and the ketone body 3-hydroxybutyrate increase in cells stimulated in Gal-medium and this is further enhanced under hypoxia (Figure S5A). $^{13}C_6$-Glc/Gal and $^{13}C_{16}$-palmitate isotope labeling *in vitro* show that $CD8^+$ T cells activated with limited Glc and/or O_2 compared to those activated in Glc-medium under normoxia have reduced carbohydrate-derived TCA cycle metabolites (Figure S5B), while more FA-derived carbons are incorporated into acetyl-CoA, TCA cycle metabolites and amino acids (Figure S5C), suggesting that FAs are increasingly used for energy and biomass production. This metabolic switch is supported by the cells' higher FA

uptake (Figure S5D) and enhanced oxidation of endogenous and exogenous FAs (Figure S5E).

We characterized the metabolism of $CD8^+$ T cells *in vivo* by isotope labeling. Mice bearing 3-day tumors were vaccinated with AdC68-gDMelapoly and AdC68-gDE7. They were given $^{13}C_6$-Glc or $^{13}C_{16}$-palmitate 14 or 30 days later. The intensity of glycolysis intermediates declines (Figure 4C, 4D) while acylcarnitine species and ketone bodies increase in $CD44^+CD8^+$ T cells from day 30 compared to day 14 tumors (Figure 4E, 4F). The relative incorporation of $^{13}C_{16}$-palmitate-dervied carbons into TCA cycle metabolites increases while that of carbons derived from $^{13}C_6$-Glc declines comparing TILs from late to early stage tumors or T cells from tumors to spleens (Figure 4G), confirming that TILs progressively enhance FA catabolism. In splenic $CD44^+CD8^+$ T cells the relative contribution of FA-derived carbon to TCA cycle metabolites remains stable or decreases over time (Figure 4G).

In the OT-1 cell transfer model, activated $CD8^+$ TILs from advanced tumors compared to those from day 14 tumors or day 30 spleens display markedly higher levels of $^{13}C_{16}$-FA-derived carbon incorporation into TCA cycle metabolites and palmitoylcarnitine (Figure 4H). In addition, the intensities of palmitoylcarnitine and ketone bodies are significantly higher in OT-1 TILs from day 30 $B16_{OVA}$ tumors (Figure 4I), further validating that the metabolic switch towards enhanced FA catabolism during tumor progression is not limited to vaccine-induced TILs. We confirmed that sample processing does not affect the profile of isotopic labeling in T cells, as shown by the nearly identical $^{13}C_{16}$-FA-derived carbon incorporation into TCA cycle metabolites from lymph node (LN) samples snap frozen on dry ice or processed into single cell suspensions and kept on ice for the time needed for sample processing (Figure S5F).

The metabolic switch of TILs is facilitated by enhanced uptake of FAs (Figure S5G) and increased expression of the FA β-oxidation (FAO) rate-limiting enzyme Cpt1a (Figure S5H) in vaccine-induced $CD8^+$ TILs from late-stage tumors. This switch is not caused by their differentiation towards memory as evidenced by low levels of CD62L (Figure S5I). The enhanced FA catabolism in TILs is further supported by increasingly high abundance of free FAs within the interstitial fluid of $B16Braf_{V600E}$ tumors (Figure 4J). Increases of different FAs in the tumor interstitial fluid during tumor progression appears to be common as it is also observed in melanoma patient-derived xenografts (PDX) from NSG mice (Figure 4K) and in fresh human melanoma metastases that were tested against human sera (Figure 4L). We also compared different FA species within the interstitial fluid of PDX tumors to those within solid organs or serum and found that a number of FA species are markedly higher within the tumors (Figure S5J).

We tested whether $CD8^+$ TILs isolated from melanoma patients display enhanced reliance on FA catabolism. Lymphocytes from blood of healthy donors or resected melanoma metastases were stained and gated onto naive, effector, effector memory (TEM) and central memory (TCM) $CD8^+$ T cell subsets (Figure 5A). Compared to circulating $CD8^+$ T cells, $CD8^+$ TILs show increases in TEMs and decreases in naive and effector cells (Figure 5B). We analyzed each T cell subset for PD-1 expression and parameters indicative of FA

catabolism. Antigen-experienced TILs show higher PD-1 levels than $CD8^+$ T cells from blood (Figure 5C). TEM and TCM $CD8^+$ TILs express higher levels of PPAR-α and Cpt1a compared to the corresponding peripheral blood mononuclear cell (PBMC) populations. Moreover, all TIL subsets show enhanced FA uptake. Collectively, our data suggest that a metabolic switch towards enhanced FA catabolism also occurs in TILs of melanoma patients.

Treatment with α-PD-1 slows tumor progression without changing $CD8^+$ TIL metabolism or functions

In clinical trials, monoclonal (m) antibodies (Ab) to PD-1 can delay tumor progression (Hamid et al., 2013; Larkin et al., 2015). As in our model $CD8^+$ TILs increase PD-1 over time, we tested if treatment with an anti-PD-1 mAb (α-PD-1) affects their metabolism or functions. Tumor-bearing mice were vaccinated and treated with α-PD-1 or an isotype control. α-PD-1 reduces PD-1 staining when the same antibody (29F.1A12) is used for treatment and detection but not upon staining with Ab RMP1-30, which is directed to a different PD-1 epitope (Figure 6A). α-PD-1 treatment enhances Phospho-Akt levels (Figure 6A), indicating it blocks the binding of PD-L1/PD-L2 to PD-1 (Patsoukis et al., 2013) without affecting the differentiation (Figure S6), metabolism (Figure 6B) or functions of TA-specific $CD8^+$ TILs (Figure 6C). It delays tumor progression in vaccinated, unvaccinated or immune-deficient NSG mice (Figure 6D).

$B16Braf_{V600E}$ tumor cells express low levels of PD-1 but are highly positive for PD-L1 (Figure 6E). To assess whether α-PD-1 treatment induces tumor cell death in a PD-L1-dependent manner (Azuma et al., 2008), we knocked-down PD-L1 in tumor cells (Figure 6F). PD-$L1^{hi}$ or PD-$L1^{lo}$ tumor cells were mixed in a 1:1 ratio and injected intraperitoneally (i.p.) into naive C57Bl/6 mice or mice that had been vaccinated 14 days earlier with Ad-gDMelapoly. Mice of each group were treated with α-PD-1 or isotype Ab prior to tumor cell challenge. Cells were isolated from the peritoneal cavity 1 day later. In isotype-treated unvaccinated or vaccinated mice, most of the recovered tumor cells are PD-$L1^{hi}$ (Figure 6G), suggesting that PD-L1 provides tumor cells with a survival advantage. Upon α-PD-1 treatment both PD-$L1^{hi}$ and PD-$L1^{lo}$ cells are recovered at equal levels, indicating the gain in survival of PD-$L1^{hi}$ cells requires back signaling through PD-1. $B16_{OVA}$ tumors are also PD-1^{lo} but positive for PD-L1 (Figure 6H). After PD-L1 KD (Figure 6I), equal numbers of PD-$L1^{hi}$ and PD-$L1^{lo}$ $B16_{OVA}$ cells were transferred into α-PD-1- or isotype Ab-treated mice that also received *in vitro* activated OT-1 $CD8^+$ T cells. The PD-$L1^{hi}$ tumor cells again show a survival advantage in the isotype Ab-treated group, which is abrogated in presence of α-PD-1 (Figure 6J). Therefore, in our models PD-1 blockade reduces tumor progression in a T cell-independent, PD-L1-dependent manner.

Enhanced reliance on FA catabolism is essential to maintain $CD8^+$ TIL functions

To further assess the impact of FA catabolism on $CD8^+$ T cell functions, we stimulated $CD8^+$ T cell in presence of fenofibrate (FF), a PPAR-α agonist that increases FA catabolism, or etomoxir (ETO), an irreversible inhibitor of Cpt1 that decreases mitochondrial FAO (Figure S7A). Addition of the drugs does not affect $CD8^+$ cells survival under the chosen experimental conditions (Figure S7B). *In vitro* FF-treated cells stimulated in Glc or Gal-

medium compared to diluent-treated cells increase FA catabolism as shown by their transcriptional profile (Figure S7C) and increased FA uptake (Figure S7D). ETO decreases OCR of $CD8^+$ T cells stimulated in either Glc- or Gal-medium (Figure S7E). OCR declines most in cells cultured with Gal under hypoxia, again confirming their increased reliance on FAO. Under hypoxia, PD-1 expression increases with FF but decreases with ETO (Figure S7F). FF increases while ETO decreases functions and polyfunctionality of $CD8^+$ T cell cultured under hypoglycemia and hypoxia (Figure S7G).

To assess how increased FA catabolism affects $CD8^+$ TILs, we vaccinated $CD90.2^+$ mice congenic for CD45, and treated them with FF (CD45.1 mice) or diluent (CD45.2 mice). Splenocytes were mixed at a 1:1 ratio of MAA-specific $CD8^+$ T cells from the 2 sets of donors and transferred into vaccinated, tumor-bearing $CD90.1^+$ recipients (Figure 7A). Prior to transfer, lymphocytes from FF-treated mice show significantly increased $^{13}C_{16}$-palmitate catabolism and higher ketone body intensity compared to those from controls (Figure S7H, S7I), validating the FF effect *in vivo*. FF-treated splenocytes show enhanced OCR, which is blocked by ETO, further confirming that FF enhances FAO (Figure S7J). Donor-derived MAA- and E7-specific $CD8^+$ T cells from mice treated with FF or diluent show comparable expression of differentiation markers, indicating that FF does not overtly affect memory formation (Figure S7K). FF-treated cells concurrently increase PD-1 and T-bet (Figure S7L) and show trends towards higher functions (Figure S7M). Donor-derived specific $CD8^+$ TILs were analyzed 3 weeks after transfer (Figure 7B). Compared to diluent-treated $CD44^+CD8^+$ TILs, those treated with FF show enhanced transcripts for factors involved in FA catabolism (Figure 7C). Both MAA- and E7-specific FF-treated $CD8^+$ TILs show trends of increased PD-1 (Figure 7D), and their frequencies and functions are significantly higher compared to those of controls (Figure 7E). Upon transfer of splenocytes from FF- or diluent-treated mice into separate cohorts of tumor-bearing hosts, the former significantly delay tumor progression (Figure 7F), confirming that enhanced FA catabolism improves $CD8^+$ TILs' functions.

To test if FF-induced increases in PD-1 affect $CD8^+$ TIL functions, we fed vaccinated donor mice with FF or diluent. Upon transfer of splenocytes into separate groups of tumor-bearing mice, we treated the recipients with α-PD-1 or the isotype control (Figure 7G). Both FF treatment of donors and α-PD-1 treatment of recipients delay tumor progression; they act synergistically and together completely prevent tumor growth in 50% of vaccinated mice (Figure 7H). α-PD-1 reduces PD-1 staining with 29F.1A12 on donor cells and this is not affected by FF (Figure S7N). PD-1 blockade only has subtle effects on functions of MAA-specific $CD8^+$ TILs derived from either set of donor mice (Figure 7I) but significantly increases frequencies of monofunctional E7-specific $CD8^+$ TILs derived from FF treated donors. This may partially reflect the smaller tumor sizes in α-PD-1 treated mice, which might primarily benefit bystander TILs.

In the cell transfer model, treatment of OT-1 cells with FF or diluent during their *in vitro* stimulation confirms that the PPAR-α agonist promotes FA catabolism as evidenced by increases in transcripts of factors involved in this process (Figure S7O). FF-treated OT-1 T cells augment FA uptake and PPARα expression (Figure S7P). FF treatment does not change T cell differentiation but significantly enhances PD-1 (Figure S7Q). It increases GrmB but

decreases IFN-γ production (Figure S7R). Within day 20 tumors, FF- or diluent-treated donor-derived OT-1 TILs show comparable PD-1 (Figure 7J). Frequencies of $GrmB^+$ and/or IFN-γ^+ donor $CD8^+$ TILs increase upon FF pre-treatment (Figure 7K) and tumor progression is markedly delayed (Figure 7L).

To further study the effects of FA catabolism, we stimulated $CD8^+$ T cells from PPAR-α knockout (KO) mice *in vitro* and compared them to those from wild type (WT) mice. Transcripts for most factors involved in the TCA cycle and lipid metabolism are higher in PPAR-α KO compared to WT $CD8^+$ T cells when stimulated in Glc-medium under hypoxia (Figure 8A). This profile reverses in cells cultured in Gal-medium with low O_2, suggesting that knocking out PPAR-α significantly decreases FA catabolism in Glc-deprived $CD8^+$ T cells. PPAR-α KO $CD8^+$ T cells cultured with limited Glc express less PD-1 than WT cells (Figure 8B) and exhibit lower functions and polyfunctions (Figure 8C). These data suggest that FA catabolism is required to maintain $CD8^+$ T cell function when access to Glc is limited.

We explored the effect of reduced FA catabolism on vaccine-induced TILs in an adoptive transfer system, in which splenocytes from vaccinated PPAR-α KO and WT mice were mixed at a 1:1 ratio of MAA-specific $CD8^+$ T cells and co-transferred into tumor-bearing, vaccinated recipients (Figure 8D). Prior to transfer, expression of CD127 (Figure S8A) and other differentiation markers (**not shown**) are similar between the two T cell subsets. Similarly, functions and polyfunctionality of MAA-specific $CD8^+$ T cells are comparable between the two groups, while E7-specfic $CD8^+$ T cells are less abundant and polyfunctional in PPAR-α KO mice (Figure S8B). This difference may reflect that strength of T cell receptor signaling, which is lower for the E7 epitope, affects the T cells' differentiation (Kaech and Cui, 2012) and thereby their metabolism (O'Sullivan et al., 2014). Within 3-week tumors, PPAR-α KO compared to WT donor-derived $CD44^+CD8^+$ TILs show a transcriptional profile indicative of reduced FA catabolism (Figure 8E). Vaccine-induced, donor-derived PPAR-α KO $CD8^+$ TILs have less PD-1 (Figure 8F) and lower functions including polyfunctions compared to those of WT controls (Figure 8G). Collectively these data confirm that PPAR-α-promoted FA catabolism preserves effector functions of $CD8^+$ TILs.

DISCUSSION

Within the TME $CD8^+$ T cells experience hypoxia and must compete for nutrients especially Glc. Recent studies report that hypoglycemia within the TME impairs $CD8^+$ T cells functions and reduces the efficacy of active immunotherapy (Chang et al., 2015; Ho et al., 2015). Our results show that metabolic stress within the TME impairs the performance of $CD8^+$ TILs including bystander TILs, although TA-specific $CD8^+$ TILs tend to be more affected, presumably for they continue to respond to stimulatory signals and may penetrate more deeply into tumors where nutrients and O_2 are especially limiting.

Melanoma develops areas of hypoxia, which activates the HIF-1α pathway in cells of the TME. HIF-1α expression also rises upon T cell activation. In our study HIF-1α increases in both MAA-specific and bystander $CD8^+$ TILs, pointing towards hypoxia as the underlying

cause. The effect of hypoxia and HIF-1α on $CD8^+$ T cells is controversial. Some studies show that O_2 is required for T cell activation and effector functions, and HIF-1α functions as a negative regulator of T cell responses (Ohta et al., 2011; McNamee et al., 2013). Others using protocols in which $CD8^+$ T cells were subjected to hypoxia during a resting period or testing cells lacking the von Hippel–Lindau tumor suppressor report that hypoxia or HIF-1α signaling increase functions (Doedens et al., 2013; Finlay et al., 2012). Our data agree with the former as they show reduced HIF-1α signaling improves the functions of activated $CD8^+$ T cells experiencing hypoxia *in vitro* or within the TME, and increases the efficacy of TA-specific $CD8^+$ T cells to delay tumor progression. These data imply that when Glc is limiting, promoting glycolysis and inhibiting OXPHOS by HIF-1α becomes detrimental to $CD8^+$ TILs. LAG-3, which according to our data is up-regulated by HIF-1α, inhibits T cell expansion and effector functions (Grosso et al., 2007). The LAG-3 locus has several HIF-1α response elements ([A/G]CGTA), which may influence LAG-3 expression.

Hypoxia and hypoglycemia send opposing metabolic signals. The former promotes glycolysis while the latter forces cells to use OXPHOS, which can be fueled by various nutrients but requires O_2. Cancer cells increase *de novo* lipogenesis (Menendez and Lupu, 2007) and recruit adipose progenitor cells. In our models including mouse and human melanomas, the abundance of free FA species increases during tumor progression, which could activate PPARα signaling in $CD8^+$ TILs, facilitate their switch towards FA catabolism and preserve their effector functions. Energy production through FAO rather than glycolysis comes at a price; more O_2 is needed to generate equivalent amounts of ATP and ROS production increases. Generating energy through FAO within a hypoxic TME may thus not be the only method by which $CD8^+$ TILs maintain their functions. Ketone bodies are highly efficient fuels that require less O_2 (Veech, 2004). They serve as a preferred energy source for cells of the nervous system subjected to hypoxia and hypoglycemia (Takahashi et al., 2014). Ketone bodies could be synthesized and secreted by other cells (Martinez-Outschoorn et al., 2012), or they could be produced by TILs directly as suggested by increased transcript levels of Bdh1, a key enzyme in ketone body metabolism, and enhanced intensities of ketone bodies in $CD8^+$ TILs from late-stage tumors. We hypothesize that ketone bodies may serve as a nutrient source for $CD8^+$ TILs, although this remains to be investigated further. We would also like to point out that levels of O_2 differ within a tumor and as TILs can randomly migrate within the TME (Mrass et al., 2006) they may use FAO and ketone bodies alternatively depending on surrounding O_2 levels.

In addition to contributing to energy production, FA catabolism could improve T cell functions through alternative pathways. When Glc is limited, FAs are used for amino acid synthesis thus promoting production of effector molecules. In addition, FAs are increasingly converted to acetyl-CoA, which can acetylate key enzymes in the TCA cycle and glycolysis pathways such as GAPDH. Acetylation increases GAPDH's enzymatic activity and reduces its binding to the 3′UTR region of IFN-γ mRNA, thus enhancing IFN-γ production (Balmer et al., 2016) and T cell effector functions.

High expression of PD-1 is viewed to signal $CD8^+$ T cell exhaustion and loss of effector functions. Our results suggest that high PD-1 expression is not inevitably linked to impaired T cell functions. Hypoxia-decreased PD-1 expression is associated with impaired functions,

while FF-treated $CD8^+$ T cells show a trend towards increased PD-1 expressions but their functions improve. PD-1 signaling inhibits TCR- and CD28-mediated activation of the PI3K/AKT/mTOR pathway, which in turn decreases glycolysis (Parry et al., 2005) and promotes lipolysis and FAO (Patsoukis et al., 2015). Enhanced PD-1 signaling in $CD8^+$ TILs might thus facilitate the $CD8^+$ TILs metabolic switch within a Glc-poor TME. In our model blockade of PD-1 after the initial phase of T cell activation affects neither metabolism nor effector functions of TILs. These results differ from those of a recent study in a mouse sarcoma model, which reports improved glycolysis and IFN-γ production by $CD8^+$ TILs treated with α-PD-1 during their initial activation (Chang et al., 2015). We assume that these apparently opposing results reflect intrinsic differences in tumor models. Alternatively, differences in timing of treatment may affect the results. PD-1 blockade during the initial stages of T cell activation may allow them to better compete for Glc within a TME; once TILs have switched to FA catabolism they remain committed to this pathway regardless of PD-1 signaling.

Our data show that PD-1 blockade may promote MAA-specific $CD8^+$ T cell infiltration into tumors (not shown). However, as α-PD-1 treatment also delays tumor progression in immune-deficient mice, we assume that it acts directly on tumors. The mouse melanoma cells in our models express low levels of PD-1 but are positive for PD-L1. *In vivo* PD-$L1^{hi}$ tumor cells have a survival advantage over PD-$L1^{lo}$ cells presumably due to back signaling upon binding to PD-1 expressed on T cells or innate immune cells. This ‘molecular shield’ is obstructed by the α-PD-1 mAb, which could thus enhance the tumor cells’ vulnerability to apoptosis or, in immunocompetent mice, indirectly improve TIL functions by increasing the tumor cells’ susceptibility to lytic enzymes (Azuma et al., 2008; Chen and Han, 2015).

Our results indicate that metabolic reprogramming of $CD8^+$ T cells to increase energy production through FA catabolism prior to adoptive cell transfer might enhance the overall efficacy of cell therapy in patients with cancers characterized by low Glc content. We further show that this metabolic manipulations improves treatment outcome upon PD-1 blockade, which is in agreement with the synergistic effect of anti-PD-1 treatment with chemicals that activate mitochondrial functions (Chamoto et al., 2017). Similarly, other studies show that memory $CD8^+$ T cells, which prefer FAO and OXPHOS for energy production, more efficiently slow tumor progression than effector cells (Crompton et al., 2015; Sukumar et al., 2013). In contrast, others report that increasing the TILs’ ability to use glycolysis improves their antitumor effect (Chang et al., 2015). Which metabolic manipulations are most suited to improve TIL-mediated tumor regression will likely depend on the nature of the tumor. Those with sufficient levels of Glc may benefit from $CD8^+$ T cells with high glycolytic potential, while tumors with a hypoglycemic TME may best be combated by $CD8^+$ T cells that favor FA catabolism.

Our *in vivo* studies focus on vaccine-induced $CD8^+$ T cells or adoptively transferred TA-specific $CD8^+$ T cells. The latter may serve as a model for *in vitro* expanded TILs or T cells with a chimeric antigen receptor, which upon adoptive transfer will encounter similar challenges within the TME and might thus benefit from metabolic reprogramming. Although most of our studies were conducted in mice, we confirm that T cells isolated from human melanoma metastases show evidence of enhanced FA catabolism, which could be fueled by

the increased levels of FAs within tumor interstitial fluid. This indicates that our results are relevant for cancer patients. Our study invites clinical investigations into the use of metabolic manipulations to improve the outcome of cancer immunotherapy.

STAR METHODS

KEY RESOURCES TABLE

REAGENT or RESOURCE	SOURCE	IDENTIFIER
Antibodies		
Rat anti-mouse PD-1 (clone 29F.1A12)	Gordon Freeman	N/A
Rat IgG2a isotype control (clone 2A3)	Bio X Cell	Cat#BE0089
Hamster anti-mouse CD3e (clone 145-2C11)	BD Biosciences	Cat#553057
Hamster anti-mouse CD28 (clone 37.51)	BD Biosciences	Cat#553294
Anti-mouse CD8a PerCP/Cy5.5 (clone 53-6.7)	Biolegend	Cat#100734
Anti-mouse CD8a Alexa Fluor 700 (clone 53-6.7)	Biolegend	Cat#100730
Anti-mouse CD4 PerCP/Cy5.5 (clone GK1.5)	Biolegend	Cat#100434
Anti-mouse/human CD44 Pacific Blue (clone IM7)	Biolegend	Cat#103020
Anti-mouse/human CD44 PerCP/Cy5.5 (clone IM7)	Biolegend	Cat#103032
Anti-mouse CD279 (PD-1) PE/Cy7 (clone RMP1-30)	Biolegend	Cat#109110
Anti-mouse CD279 (PD-1) Brilliant Violet 605 (clone 29F.1A12)	Biolegend	Cat#135220
Anti-mouse CD274 (PD-L1) APC (clone 10F.9G2)	Biolegend	Cat#124312
PE/Cy7 Rat IgG2b, κ Isotype Ctrl (clone RTK4530)	Biolegend	Cat#400617
APC Rat IgG2b, κ Isotype Ctrl (clone RTK4530)	Biolegend	Cat#400611
Anti-mouse CD223 (LAG-3) APC (clone C9B7W)	Biolegend	Cat#125210
Anti-mouse CD223 (LAG-3) PerCP/Cy5.5 (clone C9B7W)	Biolegend	Cat#125212
Anti-mouse CD127 Brilliant Violet 421 (clone A7R34)	Biolegend	Cat#135027
Anti-mouse CD127 Alexa Fluor 700 (clone A7R34)	eBioscience	Cat#56-1271-82
Anti-mouse CD62L FITC (clone MEL-14)	Biolegend	Cat#104406
Anti-mouse CD62L Brilliant Violet 785 (clone MEL-14)	Biolegend	Cat#104440
Anti-mouse/human KLRG1 PE/Cy7 (clone 2F1/KLRG1)	Biolegend	Cat#138416
Anti-mouse TCR Vα2 PE (cloneB20.1)	Biolegend	Cat#127808
Anti-rat CD90/mouse CD90.1 (Thy1.1) PerCP/Cy5.5 (clone OX-7)	Biolegend	Cat#202515
Anti-rat CD90/mouse CD90.1 (Thy1.1) APC (clone OX-7)	Biolegend	Cat#202526
Anti-mouse CD45.1 Pacific Blue (clone A20)	BD Bioscience	Cat#110722
Anti-human CD3 PerCP/Cy5.5 (clone SP34-2)	BD Bioscience	Cat#552852
Anti-human CD8 APC-H7 (clone SK1)	BD Bioscience	Cat#560179
Anti-human CD14 Pacific Blue (clone M5E2)	BD Bioscience	Cat#558121
Anti-human CD19 Pacific Blue (clone HIB19)	Biolegend	Cat#302224
Anti-human CD28 PE/Texas Red (clone CD28.2)	Beckman Coulter	Cat#6607111
Anti-human CD95 (Fas) PE/Cy5 (clone Dx2)	BD Bioscience	Cat#559773
Anti-human CCR7 PE (clone 150503)	R&D Systems	Cat#FAB197P
Anti-human PD-1 PE/Cy7 (clone EH12.2H7)	Biolegend	Cat#329918
Anti-T-bet PE/Cy7 (clone 4B10)	eBioscience	Cat#25-5825-82
Anti-EOMES (clone Dan11mag)	eBioscience	Cat#53-4875-82
Anti-mouse IFN-γ □□□ (clone XMG1.2)	Biolegend	Cat#505810
Anti-mouse IFN-γ Brilliant Violet 421 (clone XMG1.2)	Biolegend	Cat#505830
Anti-Granzyme B APC (clone GB12)	ThermoFisher	Cat#MHGB05
Anti-Perforin PE (clone eBioOMAK-D)	ThermoFisher	Cat#12-9392-82
Anti-FoxO1 Rabbit mAb (clone C29H4)	Cell Signaling Technology	Cat#2880S

Anti-rabbit IgG (H+L), F(ab')2 Fragment Alexa Fluor 647	Cell Signaling Technology	Cat#4414S
Anti-CPT1A Alexa Fluor 488 (clone 8F6AE9)	Abcam	Cat#ab171449
Mouse IgG2b, κ Isotype Ctrl Alexa Fluor 488 (clone 7E10G10)	Abcam	Cat#ab171465
Anti-PPAR alpha Biotin	Abcam	Cat#ab48369
Streptavidin Brilliant Violet 605	Biolegend	Cat#405229
Anti-AKT [p Ser473] Alexa Fluor 488 (clone 545007)	Novus	Cat#IC7794G
Anti-human/mouse HIF-1α Alexa Fluor 700 (clone 241812)	R&D Systems	Cat#IC1935N
Anti-glucose transporter Glut1 Alexa Fluor 488 (clone EPR3915)	Abcam	Cat#195359
Mouse IgG1 Alexa Fluor 700, κ Isotype Ctrl (clone 11711)	R&D Systems	Cat#IC002N
Rabbit IgG, monoclonal isotype ctrl Alexa Fluor 488 (clone EPR25A)	Abcam	Cat#ab199091
Bacterial and Virus Strains		
AdC68-gD	This paper	N/A
AdC68-gDMelapoly	This paper	N/A
AdC68-gDE7	Lasaro MO et al., 2008	N/A
Lentiviral-shHIF-1αE1674-Thy1.1	This paper	N/A
Lentiviral-shHIF-1αE1676-Thy1.1	This paper	N/A
Lentiviral-shHIF-1αE1677-Thy1.1	This paper	N/A
Lentiviral-scramble shRNA-Thy1.1	This paper	N/A
Lentiviral-shPDL1505-TurboGFP	This paper	N/A
Lentiviral-shPDL1035-TurboGFP	This paper	N/A
Lentiviral-shPDL1409-TurboGFP	This paper	N/A
Lentiviral-shPDL1141-TurboGFP	This paper	N/A
Lentiviral-non-silencing shRNA-TurboGFP	This paper	N/A
Biological Samples		
Human serum samples	Clinical Research Unit, Duke University Medical Center	N/A
Human PBMC samples	Clinical Research Unit, Duke University Medical Center	N/A
Human melanoma metastases samples	Hospital of University of Pennsylvania	N/A
Patient-derived xenograft	Hospital of University of Pennsylvania	N/A
Chemicals, Peptides, and Recombinant Proteins		
BODIPY FL C_{16}	ThermoFisher	Cat#D3821
DiOC6(3) (3,3'- Dihexyloxacarbocyanine Iodide)	ThermoFisher	Cat#D273
MitoSOX Red Mitochondrial Superoxide Indicator	ThermoFisher	Cat#M36008
Trp-1_{455}-tetramer-PE (H-2D^b, TAPDNLGYM)	NIAID	N/A
E7-tetramer-Alexa647 (H-2D^b, RAHYNIVTTF)	NIAID	N/A
OVA-tetramer-Alexa647 (H-2K^b, SIINFEKL)	NIAID	N/A
Protein Transport Inhibitor (Containing Brefeldin A)	BD Biosciences	Cat#555029

Phorbol 12-myristate 13-acetate (PMA)	Sigma-Aldrich	Cat#P8139
Ionomycin calcium salt	Sigma-Aldrich	Cat#13909
(+)-Etomoxir sodium salt hydrate	Sigma-Aldrich	Cat#E1905
Fenofibrate	Sigma-Aldrich	Cat#F6020
2-Deoxy-D-glucose	Sigma-Aldrich	Cat#D8375
MitoTEMPO	Sigma-Aldrich	Cat#SML0737
Rotenone	Sigma-Aldrich	Cat#R8875
Antimycin A	Sigma-Aldrich	Cat#A8674
Oligomycin A	Sigma-Aldrich	Cat#75351
L-Carnitine	Sigma-Aldrich	Cat#C0158
Carbonyl cyanide 4-(trifluoromethoxy) phenylhydrazone (FCCP)	Sigma-Aldrich	Cat#C2920
Bovine Serum Albumin, fatty acid free	Sigma-Aldrich	Cat#A8806
Cobalt (II) chloride hexahydrate	Sigma-Aldrich	Cat#202185
Fetal Bovine Serum, Dialyzed	Sigma-Aldrich	Cat#F0392
Fetal Bovine Serum, Dialyzed	Sigma-Aldrich	Cat#F0392
Polybrene	Sigma-Aldrich	Cat#TR-1003
Potassium palmitate-$^{13}C_{16}$	Sigma-Aldrich	Cat#605751
D-Glucose(U-$^{13}C_6$, 99%)	Cambridge Isotope Laboratories	Cat#CLM-1396
GlutaMAX Supplement	ThermoFisher	Cat#35050061
Seahorse XF Palmitate-BSA FAO Substrate	Agilent	Cat#102720-100
Peptide mTrp-$1_{455-463}$: TAPDNLGYA	Genscript	N/A
Peptide mTrp-$1_{481-489}$: IAVVAALLL	Genscript	N/A
Peptide mTrp-$2_{522-529}$: YAEDYEEL	Genscript	N/A
Peptide hTp-$2_{180-188}$: SVYDFFVWL	Genscript	N/A
Peptide hTrp-$2_{343-357}$: STFSFRNAL	Genscript	N/A
Peptide mTrp-$2_{363-371}$: SQVMNLHNL	Genscript	N/A
Peptide hgp100_{25-33}: KVPRNQDWL	Genscript	N/A
Peptide mBraf $_{594-602}$: FGLANEKSI	Genscript	N/A
Peptide for E7 epitope: RAHYNIVTTF	Genscript	N/A
Peptide for OVA epitope: SIINFEKL	Genscript	N/A
Critical Commercial Assays		
FITC BrdU flow kit	ThermoFisher	Cat#BDB559619
LIVE/DEAD fixable aqua dead cell stain kit	ThermoFisher	Cat#L34957
CellTrace Violet cell proliferation kit	ThermoFisher	Cat#C34557
$CD8^+$ T cell isolation kit, mouse	Miltenyl Biotec	Cat#130-104-075
Dead cell removal kit	Miltenyl Biotec	Cat#130-090-101
CD90.1 Microbeads, mouse and rat	Miltenyl Biotec	Cat#130-094-523
RNeasy Mini kit	Qiagen	Cat#74106
RNeasy Micro kit	Qiagen	Cat#74004
Calcium Phosphate transfection kit	ThermoFisher	Cat#K278001
Foxp3/Transcription Factor Staining Buffer Set	eBioscience	Cat#00-5523-00
Fix Buffer I	BD Bioscience	Cat#557870
Perm Buffer III	BD Bioscience	Cat#558050
Fixation/Permeabilization Solution Kit	BD Bioscience	Cat#554715

Seahorse XF Cell Mito Stress Test Kit	Agilent	Cat#103015-100
Seahorse XF Glycolysis Stress Test Kit	Agilent	Cat#103020-100
Experimental Models: Cell Lines		
B16Braf$_{V600E}$ cells	Meenhard Herlyn	N/A
B16$_{OVA}$ cells	Richard Dutton	N/A
HEK 293 cells	ATCC	CRL-1573
293T cells	ATCC	CRL-3216
Experimental Models: Organisms/Strains		
Mice: C57BL/6	The Jackson Laboratory	Strain: 000664
Mice: C57BL/6	Charles River/NCI	Strain code: 556
Mice: B6.SJL-Ptprc^{a}Pepc^{b}/BoyJ	The Jackson Laboratory	Strain: 002014
Mice: B6.PL-*Thy*1^{a}/CyJ	The Jackson Laboratory	Strain: 000406
Mice: 129S4-*Ppara*^{tm1Gonz}/J	The Jackson Laboratory	Strain: 003580
Mice: C57Bl/6-Tg(TcraTcrb)1100Mjb/J	The Jackson Laboratory	Strain: 003831
Mice: NOD.Cg-Prkdc^{scid}Il2rg^{tm1Wjl}/SzJ	The Jackson Laboratory	Strain: 005557
Oligonucleotides		
Primers for analysis of transcripts of factors involved in nutrient metabolism, see Table S1	IDT	N/A
Recombinant DNA		
pAdC68-gD	This paper	N/A
pAdC68-gDMelapoly	This paper	N/A
pAdC68-gDE7	Lasaro MO et al., 2008	N/A
pLKO.1-shHIF-1αE1674	RNAi Consortium	TCR#: TRCN0000054448
pLKO.1-shHIF-1αE1676	RNAi Consortium	TCR#: TRCN0000054450
pLKO.1-shHIF-1αE1677	RNAi Consortium	TCR#: TRCN0000054451
pLKO.1-scramble shRNA	Addgene	Addgene plasmid#1864
pLKO.3-Thy1.1	Addgene	Addgene plasmid#14749
psPAX2	Addgene	Addgene plasmid#12260
pMD2.G	Addgene	Addgene plasmid#12259
pLKO.1-shHIF-1αE1674-Thy1.1	This paper	N/A
pLKO.1-shHIF-1αE1676-Thy1.1	This paper	N/A
pLKO.1-shHIF-1αE1677-Thy1.1	This paper	N/A
pLKO.1-scramble shRNA-Thy1.1	This paper	N/A
pGIPZ-shPDL1505-TurboGFP	Dharmacon	Dharmacon#: RMM4531-200414505 V3LMM_437373

pGIPZ-shPDL1035-TurboGFP	Dharmacon	Dharmacon#: RMM4531-200331035 V2LMM_71093
pGIPZ-shPDL1409-TurboGFP	Dharmacon	Dharmacon#: RMM4531-200312409 V2LMM_62208
pGIPZ-shPDL1141-TurboGFP	Dharmacon	Dharmacon#: RMM4531-200114141 V3LMM_437377
pGIPZ-non-silencing shRNA-TurboGFP	Dharmacon	Cat#RHS4346
Software and Algorithms		
Graphpad Prism 6.0 software	GraphPad Software, Inc.	http://www.graphpad.com/scientificsoftware/prism/
FlowJo software 9.9.5	FlowJO, LLC	https://www.flowjo.com/
PAPROC I	University of Tübingen, Department of Biomathematics and Department of Immunology	http://www.paproc2.de/paproc1/paproc1.html
Netchop 3.1	Technical Univesity of Denmark, Center for Biological Sequence Analysis	http://www.cbs.dtu.dk/services/NetChop/
IEBD Analysis Resource	NIAID	http://tools.immuneepitope.org/main/

CONTACT FOR REAGENT AND RESOURCE SHARING

Further information and requests for resources and reagents should be directed to and will be fulfilled according to institutional rules by the Lead Contact, Hildegund Ertl (ertl@wistar.org).

EXPERIMENTAL MODEL AND SUGJECT DETAILS

Mice—All procedures were conducted following protocols approved by the Wistar IACUC. Female C57Bl/6, B6.SJL-Ptprc^{a}Pepc^{b}/BoyJ (B6 CD45.1^{+}), B6.PL-*Thy*1^{a}/CyJ (B6 CD90.1^{+}), B6; 129S4-*Ppara*^{tm1Gonz}/J (B6 PPAR-α KO), C57Bl/6-Tg(TcraTcrb)1100Mjb/J (OT-1) and NOD.Cg-Prkdc^{scid}Il2rg^{tm1Wjl}/SzJ (NSG) mice (6–8 weeks) were purchased from Charles River, National Cancer Institute (NCI) or Jackson Laboratories and housed at the Wistar Institute Animal Facility. Groups of 5–80 C57BL/6 mice were vaccinated intramuscularly (i.m.) with 10^{10} virus particles [vp] of AdC68-gDMelapoly, 10^{11}vp of AdC68-gDE7 or 10^{11}vp AdC68-gD. For tumor challenge experiments B16Braf$_{V600E}$ cells (5×10^{4} cells/mouse) or B16$_{OVA}$ cells (10^{5} cells/mouse) were resuspended in PBS and injected subcutaneously (s.c.) into the right flank. For PDX model, NSG mice were injected s.c. with WM4231-2 cells (10^{5} cells/mouse). The WM4231-2 cells were established from a surgically removed metastatic lesion from a patient with treatment-naive melanoma. Tumor growth was monitored by measuring the perpendicular diameters of tumors every other day. Depending on size early stage tumors were harvested 10–14 days after challenge (referred to

as day 14) while late stage tumors were harvested 4–5 weeks after challenge (referred to as day 30). For adoptive transfer in the B16Braf$_{V600E}$ tumor model, 1×10^7 *in vitro* activated CD8$^+$ T cells transduced with lentivectors were injected intravenously (i.v.) into recipient mice bearing 5 day-old tumors. For the OT-1 T cell transfer model, 2×10^6 OT-1 splenocytes or 10^6 OT-1 CD8$^+$ T cells stimulated for 4–5 days *in vitro* were transferred i.v. into mice bearing 5 day-old B16$_{OVA}$ tumors.

For *in vivo* treatment FF (100 mg/kg/day) in DMSO/PBS was given by oral gavage daily for 3 weeks. Control mice received diluent. For co-transfer experiments, splenocytes containing 10^5 MAA-specific CD8$^+$ T cells from the experimental and control groups were mixed and transferred i.v. into CD90.1$^+$ recipient mice. For FF-treated OT-1 CD8$^+$ T cell transfer, FF was added for 48 hr at 25 μM on day 4 of OT-1 T cell activation. For PD-1 blockade experiments in NSG or unvaccinated C57BL/6 mice, α-PD-1 Ab (clone 29F.1A12) or the isotype control Ab (Iso, Clone: 2A3, Bio X Cell) were given as of day 3 after tumor cell challenge. In vaccinated C57BL/6 mice, α-PD-1 or Iso treatment was started 10 days after vaccination. The Abs were given i.p. every 3rd day at a dose of 200 μg/mouse.

Patient samples—Human studies were approved by the Institutional Review Board (IRB) of the Wistar Institute (protocol 21111257, protocol 2802240-4b). Informed consent was obtained from each patient before blood or tumor tissue collection. The human blood and serum samples were obtained from clinical research unit, Duke University (Durham, NC, USA) in accordance with the local IRB. Samples were from male and female Caucasians between the ages of 32–39. Lymphocytes from periphery blood were isolated by Ficoll-Paque PLUS (GE Healthcare Biosciences) gradient using standard procedures. The PDX sample and the fresh metastatic tumors from melanoma patients were obtained from melanoma patients at the Hospital of the University of Pennsylvania upon their informed consent under protocol 2802240-4b. To ensure patient confidentiality no information on age, gender or ethnicity were provided to the investigators of this study. Metastases were cut into small pieces, digested with Collagenase/DNAse I and filtered through 70 μm cell strainers to produce single cell suspension. TILs were purified by Percoll-gradient.

Cell lines—The B16Braf$_{V600E}$ cell line was derived from B16.F10 cells by transduction with the lentivector pLU-EF1a-mCherry expressing mouse Braf$_{V600E}$. The B16$_{OVA}$ cell line was a gift from Dr. R. Dutton (Wadsworth Center, Albany, NY). HEK 293 cells were used to propagate vaccine vectors. 293T cells were used to produce lentivectors. Cells were grown in Dulbecco's Modified Eagles medium (DMEM) supplemented with 10% fetal bovine serum (FBS).

METHOD DETAILS

Construction of recombinant adenoviral vectors and lentivectors—Molecular construction, rescue, purification and titration of the adenoviral vectors have been described (Zhang and Ertl, 2014). The Melapoly sequence is composed of eight CD8$^+$ T cell epitopes from human (h) or mouse (m)Trp-2, mTrp-1, hgp100 and mBraf$_{V600E}$ fused into herpes simplex virus (HSV) glycoprotein (g)D. We design the spacers between each epitopes using PAPROCI, Netchop 3.1 and IEBD Analysis Resource. Briefly, gDMelapoly or gDE7

sequences were inserted into the E1-deleted AdC68 viral molecular clone using I-CeuI and PI-SceI restriction enzyme sites. The constructed plasmids were used to transfect HEK 293 cells by calcium phosphate (Invitrogen). Cells infected with Ad vectors were harvest 7–10 days later upon plague formation. Virus was expanded on HEK 293 cells by serial infections and harvested by three cycles of freeze thawing. Virus was purified from cell-free supernatant after the third cycle of thawing by cesium chloride density ultracentrifugation.

For production of lentivectors for HIF-1α KD, three pLKO.1 lentivectors containing shRNAs targeting different regions of HIF-1α or a pLKO.1 lentivector containing scrambled shRNA were obtained from the RNAi Consortium or Addgene. The selection marker Thy1.1 was cloned from the pLKO.3-Thy1.1 lentivector (Addgene) into each of the shRNA lentivectors. Lentivectors were generated using the 2nd generation lentivector package system (Addgene) by transfecting 293T cells with the packaging plasmid PsPAX2, the envelope plasmid PMD2.G and each of the shRNA-Thy1.1-expressing insert plasmids at a ratio of 3:1:1. Supernatants were collected 48 and 72 hr after transfection, spun at 3000rpm for 10 min and filtered through 0.45 μm filters. Lentivectors were concentrated by ultracentrifugation at 25,000 rpm, 4 °C for 2 hr. Vector pellets were incubated with PBS at 4 °C overnight before resuspension. Each lentivector, E1674, E1676 and E1677, was used to transduce activated CD8$^+$ T cells independently for *in vitro* experiments, to control for potential off-target effect. E1676 was used in the vaccine model. A mixture of three lentivectors was used to transduce activated OT-1 cells in the OT-1 cell transfer model. For PD-L1 KD, four GIPZ lentiviral mouse CD274 shRNA constructs with TurboGFP and puromycin selection markers (Dharmacon) were used to produce lentivectors. A lentivector with scrambled non-silencing shRNA was used as control. The efficiency of PD-L1 KD was compared between different vectors. Two lentivectors shPDL1505-TurboGFP and shPDL1035-TurboGFP were independently used for downstream studies with B16Braf$_{V600E}$ cells; one was selected for studies with B16$_{OVA}$ cells. Transduction with PD-L1 shRNA vectors or the control vector did not affect the growth of B16$_{OVA}$ tumor cells *in vitro*.

***In vitro* stimulation of CD8$^+$ T cells and drug treatments—**Enriched CD8$^+$ T cells from naive C57BL/6 mice were activated for 4 days in 6-well plates pre-coated with Ab to CD3 (5 μg/ml) and CD28 (1 μg/mL) (BD Bioscience). For some samples, cells were transferred for the last 16 hr to a hypoxia chamber. OT-1 splenocytes were stimulated with SIINFEKL peptide (2 μg/mL) and IL-2 (100 U/ml, Roche) for 48 hr. They were then maintained in medium containing IL-2 and split every other day. To study the impact of hypoxia on relatively resting CD8$^+$ T cells, enriched CD8$^+$ T cells were stimulated for 48 hr under normoxia. Cells were then removed from the plates, washed and replated in fresh medium with IL-2 (100 U/ml) for 96 hr, followed by culture in normoxia or hypoxia with IL-2 for another 36 hr before analysis. Cells were cultured in Roswell Park Memorial Institute (RPMI) medium without Glc (Life Technologies) supplemented with Glc (10 mM) or Gal (10 mM), 10% dialyzed FBS (Life Technologies), 20 mM HEPES, 2 mM Glutamax, 1 mM sodium pyruvate, 0.05 mM 2-mercaptoethanol and 1% penicillin-streptomycin. Hypoxia experiments were performed in a Thermo Napco series 8000WJ CO_2 incubator equipped with nitrogen tank for O_2 replacement. O_2 level was kept at 1% during hypoxia experiments for the indicated time periods. In all assays cell viability was assessed before

staining. Drugs and corresponding vehicle controls (all from Sigma) were added as follows: 2-deoxy-D-glucose (2-DG, 2 mM) or Fenofibrate (FF, 50 μM) for the entire culture period; Etomoxir (ETO, 200 μM) for the last 48 hr. FCCP (500 μM), Mito-TEMPO (500 μM) and oligomycin (1 mM) were used as positive and negative controls for mitochondrial stains. They were incubated with cells at 37 °C for 20 min before samples were stained with DiOC6 and MitoSOX Red. DMSO concentrations were kept below 0.2% for all culture conditions.

Lentivector transduction of CD8$^+$ T cells—For *in vitro* experiments, 4×10^6 enriched CD8$^+$ T cells were stimulated as described above for 24–28 hr. Freshly concentrated lentivectors were spun-inoculated into activated CD8$^+$ T cells supplemented with polybrene (6 μg/ml, Santa Cruz) at 2000 rpm, 32°C for 2 hr. For tumor cell transduction, lentivectors were incubated with tumor cells in 1ml serum-free, antibiotic-free medium and spun at 2500 rpm, 30 °C for 30 min. One ml of complete medium was added 6 hr later. Cells were washed 20 hr after transduction and stimulated for another 40 hr under normoxia or part-time hypoxia. For *in vivo* adoptive transfer experiment in the vaccine model, recipient mice had been challenged with tumor cells 5 days earlier and had been vaccinated with AdC68-gDMelapoly 2 days earlier. CD8$^+$ T cells from spleens of naive C57Bl/6 mice were purified by negative selection using magnetic beads (MACS, STEMCELL Technologies). Enriched CD8$^+$ T cells were stimulated with anti-CD3/CD28 Ab for 24 hr prior to lentivector transduction. Cells were washed 20 hr after transduction and cultured for an additional 48 hr in medium with IL-2 (100 U/ml) before transfer. For *in vivo* assays in the adoptive cell transfer model, OT-1 splenocytes were stimulated with peptide and IL-2 for 24 hr prior to spin inoculation with lentivectors. 72 hr later, dead cells were removed and transduced OT-1 CD8$^+$ T cells were further purified by positive selection using CD90.1 microbeads (Miltenyi Biotec) before cell transfer.

Isolation of lymphocytes from mice—PBMCs and lymphocytes from spleens and lymph nodes were harvested as described (Zhang and Ertl, 2014). Briefly, blood samples were collected by submandibular puncture and PBMCs were isolated by Histopaque (Sigma) gradient centrifugation. Single cell suspension was generated by mincing spleens and lymph nodes with mesh screens in Leibovitz's L15 medium followed by passing cells through a 70 μm filter (Fisher Scientific). Red blood cells were lysed by 1x RBC lysis buffer (eBioscience). To obtain tumor-infiltrating lymphocytes, tumors were harvested, cut into small fragments and treated with 2 mg/ml Collagenase P, 1 mg/ml DNase I (all from Roche) and 2% FBS (Tissue Culture Biologicals) in Hank's balanced salt solution (HBSS,1X, Thermo Fisher Scientific) under agitation for 1 hour. Tumor fragments were homogenized, filtrated through 70 μm strainers and lymphocytes were purified by Percoll-gradient centrifugation and washed with DMEM supplemented with 10% FBS. Pre-experiments were conducted to ensure that this treatment did not affect expression levels of any of the tested markers.

Ab, staining and flow cytometry—Cells were stained with a PE-labeled Trp-1-specific MHC class I (H-2D^b) tetramer carrying the TAPDNLGYM peptide, an Alexa647-labeled HPV-16 E7-specific MHC class I (H-2D^b) tetramer carrying the RAHYNIVTTF peptide or

an Alexa647-labeled OVA-specific MHC class I (H-2K^b) tetramer carrying the SIINFEKL peptide (NIAID Tetramer Facility). Lymphocytes were stained with anti-CD8-PerCPCy5.5 or -Alexa700, CD4-PerCPCy5.5, CD44-PacBlue or PerCPCy5.5, LAG-3-APC or -PerCPCy5.5, PD-1-PE-Cy7 (clone RMP1-30) or -Brilliant violet (BV) 605 (clone 29F.1A12), CD127-BV421 or -Alexa700, CD62L-FTIC or BV785, KLRG1-PE-Cy7, CD45.1-Pacific Blue, Vα2-PE and Thy1.1-PerCPCy5.5 or -APC (all from Biolegend or eBioscience) and Amcyan fluorescent reactive dye (ThermoFisher). For human PBMC or TILs analysis, cells were stained with fluorochrome-labeled Ab to CD14/CD19 (dump gate), CD3, CD8, CD95, CD28 and CCR7 to identify subsets and with Ab to PD-1, PPAR-α, Cpt-1a and BODYPY FL C_6. Levels of PD-1 and PD-L1 expression on tumor cells were determined with anti-PD-1-PE-Cy7 or anti-PD-L1-APC Ab used in comparison to isotype control Ab (Biolegend). For analysis of mitochondrial markers, cells were stained with MitoSOX Red (5μM, MROS) and DiOC6 (40nM, MMP) (ThermoFisher) at 37 °C for 30 min under normoxia or hypoxia. For fatty acid uptake experiments, cells stimulated under different conditions *in vitro* or isolated from spleen and tumors of mice bearing day 14 or day 30 tumors were immediately incubated with 1 μM BODIPY FL C_{16} (ThermoFisher) for 30 min at 37 °C. Cells were washed twice with cold PBS before surface staining. For staining of T-bet, Eomes, total FoxO1, Cpt1a or PPAR-α cells were first stained for surface markers, then fixed and permeabilized with Foxp3/Transcription factor staining buffer and stained with T-bet-PE-Cy7, Eomes-Alexa488 (all from eBioscience), primary Ab against FoxO1 (C29H4, Cell Signaling Technology), anti-Cpt1a-Alexa 488 Ab or mouse IgG2b Isotype Ab; or anti-PPAR-α Ab (Abcam). Total FoxO1 was further determined by anti-rabbit secondary Ab staining (Cell Signaling Technology). PPAR-α was further detected with Streptavidin-BV605 (Biolegend). Phorphorylated (p)Akt was detected by staining cells with BD Phosflow buffers (Fix Buffer I and Perm Buffer III) and Phospho-Akt (Novus, clone 545007) Ab to Akt phosphorylated at serine 473.

For HIF-1α and Glut staining, in *ex vivo* assays mice were perfused immediately after euthanasia with Hank's balanced salt solution (HBSS) and heparin (10 units/ml) and then with 1 mM Cobalt (II) chloride ($COCl_2$, Sigma-Aldrich) diluted in PBS. For both *ex vivo* and *in vitro* experiments, lymphocyte isolation and staining before fixation were performed in medium containing 200 μM $COCl_2$. Cells were stained with Abs to cell surface markers for 30 min. Cells were fixed and permeabilized using the FoxP3 buffer kit, and stained for HIF-1α with anti-HIF-1α-Alexa700 Ab (R&D), or anti-Glut1-Alexa488 (Abcam) and the corresponding isotype control antibodies.

For intracellular cytokine staining (ICS) of *ex vivo* stimulated lymphocytes, ~10^6 cells per samples were cultured in DMEM containing 2% FBS and Golgiplug (Fisher Scientific, 1.5 μl/ml) for 6 hr with either a peptide pool (5 ug/ml for each peptide) including all CD8$^+$ T cell epitopes expressed by gDMelapoly (mTrp-1$_{455-463}$: TAPDNLGYA, mTrp-1$_{481-489}$: IAVVAALLL, mTrp-2$_{522-529}$: YAEDYEEL, hTp-2$_{180-188}$: SVYDFFVWL, hTrp-2$_{343-357}$: STFSFRNAL, mTrp-2$_{363-371}$: SQVMNLHNL, hgp100$_{25-33}$: KVPRNQDWL, mBraf $_{594-602}$: FGLANEKSI); the E7 peptide: RAHYNIVTTF or SIINFEKL peptide (all from Genscript) or a rabies virus glycoprotein control peptide. For ICS performed with CD8$^+$ T cells activated *in vitro*, ~10^6 cells were transferred to 96 well plates in the original medium and stimulated with PMA (50 ng/ml), ionomycin (2 μg/ml) and Golgiplug for 4 hr under

normoxia or hypoxia. Cells were stained with Ab to IFN-γ (APC or BV421), GrmB (APC, Life Technologies) and perforin (PE, eBioscience) after fixation/permeabilization (BD Pharmingen). Cells were analyzed by an LSRII (BD Biosciences). Data were analyzed with FlowJo (TreeStar).

T cell assays—$CD8^+$ T cells were analyzed by tetramer staining to assess phenotypes or by intracellular cytokine staining (ICS) following a 5-hour period of peptide stimulation in presence of GolgiPlug (BD Biosciences). The dominant $CD8^+$ T response elicited by the AdC68-gDMelapoly vector is directed against the Trp-1_{455} epitope (~90% of MAA-specific $CD8^+$ T cell response), which was assessed by tetramer staining. All peptides carrying the tumor antigen-specific epitopes of the vaccine inserts were used for ICS. For easier reference in the text we refer to both types of AdC68-gDMelapoly-induced $CD8^+$ T cells as MAA-specific $CD8^+$ T cells.

***In vivo* tumor cell survival assay—**Mice were treated with isotype control- or α-PD-1 Ab (200 μg/mouse) 4 and 1 days before tumor cell challenge. Some of the mice had either been vaccinated with AdC68-gDMelapoly 14 days earlier, or been injected i.p. with *in vitro* activated OT-1 $CD8^+$ T cells (10^5 cells/mouse) 4–6 hr before tumor cell challenge. PD-$L1^{hi}$ (scrambled shRNA lentivector transduced) or PD-$L1^{lo}$ (PD-L1 shRNA lentivectors transduced) $B16Braf_{V600E}$ tumor cells or $B16_{OVA}$ cells were sorted based on lentivector GFP expression and passaged for several rounds in presence of puromycin to create transduced stable cell lines. Transduced tumor cells were labeled with high (2 μM) or low (0.2 μM) levels of CellTrace Violet (CTV), respectively, mixed at 1:1 ratio and injected i.p. into recipient mice at a dose of 10^6 cells/tumor cell subset. 1-day later mice were euthanized. Cells were collected by vigorously rinsing the peritoneal cavity with a trypsin solution. Cells were washed and stained with Ab to CD3, CD14 and CD19 as dump gates and with mAb to PD-L1. The relative recovery of CTV^{hi}PD-$L1^{hi}$ vs. CTV^{lo}PD-$L1^{lo}$ cell subsets in each treatment groups was determined by flow cytometry.

BrdU proliferation assay—Mice were injected i.p. with of BrdU (1.5–2 mg/mouse) and fed water-containing BrdU at a concentration of 0.8 mg/ml on days 9, 19 or 29 after vaccination; they were euthanized the next day and lymphocyte samples were analyzed for BrdU incorporation. Cells were first stained for surface markers and then for intracellular BrdU (1:50 dilution) according to the manufacture's instruction (ThermoFisher).

Extracellular Flux Analysis and FAO assay—OCR and ECAR for $CD8^+$ T cells stimulated under different conditions were measured with XF24 and XF96 Extracellular Flux Analyzers (Seahorse Bioscience). Hypoxia samples were prepared in a hypoxia chamber under 1% O_2. Dead cells were removed by a dead cell removal kit (Miltenyi Biotec) and live cells were pre-incubated with 100 μM $COCl_2$ before being removed from the hypoxia chamber and entered into the Seahorse analyzer. To determine the contribution of FAO to OCR, 200 μM ETO was added 15 min before the Seahorse analysis. Briefly after repeated measures of basal respiration and lactate production, 1 μM OM was added to measure ATP leakage by OCR and glycolytic capacity by ECAR. 1.5 μM FCCP was then added to measure maximal respiration by OCR followed by addition of 100 nM Rotenone

and 1 μM Antimycin A to determine spare respiratory capacity by OCR and then 100 mM 2-DG to determine glycolytic reserve by ECAR. For measuring oxidation of exogenous and endogenous FAs, cells activated in either Glc- or Gal-medium for 3 days were washed and transferred to substrate-limited Glc- or Gal-medium for overnight stimulation. Substrate limited media contained 0.5 mM Glc or Gal, 1 mM GlutaMAX, 0.5 mM carnitine (all form Sigma) and 1% dialyzed FBS. Samples were treated with either ETO or vehicle control 15 min before the assay. Palmitate: BSA or BSA was added just before the assay. The contributions of FAO to OCR was calculated as follows: Basal respiration due to exogenous FA oxidation= Basal Palm:BSA-ETO OCR rate – basal BSA-ETO OCR rate - OCR due to uncoupling by FFA; uncoupling by FFA= after OM injection, Palm:BSA-ETO OCR rate - BSA-ETO rate. Basal OCR due to endogenous FAs consumption = basal BSA-ETO OCR rate - basal BSA+ETO OCR rate.

Lipid and Glc concentration measurement in tumor or tissue interstitial fluid— Interstitial fluid from kidney, heart and mouse or human melanoma samples were collected by centrifugation as described (Wiig et al., 2003) and snap frozen on dry ice. Mice were perfused with HBSS with 10 U/ml heparin before tissue collection. Concentrations of free FA species were determined by LC-MS. Absolute concentrations of Glc were measured by LC-MS upon adding $^{13}C_6$-Glc as the internal standard.

Isotopic labeling *in vitro*—For $^{13}C_6$- Glc/Gal tracing *in vitro,* cells were cultured in Glc-free RPMI medium with 10 mM $^{13}C_6$-Glc/Gal (Sigma or Cambridge) for 4 days. For $^{13}C_{16}$-palmitate tracing *in vitro,* cells were stimulated for 3 days in Glc- or Gal-medium. On the night of day 3, some samples were transferred to 1% O_2 for overnight culture. $^{13}C_{16}$-palmitate (Sigma) was first dissolved in 100% ethanol at 200 mM and conjugate to fatty acid-free BSA at a 5:1 molar ratio to a final concentration of 8 mM-$^{13}C_{16}$-palmitate-BSA by vortexing at 37 °C for 3–4 hr with sonication. On day 4, samples were pelleted and replated in fresh medium with 10% delipidated FBS (Cocalico Biologicals) and 400 μM $^{13}C_{16}$-palmitate-BSA. Hypoxia samples were returned to 1% O_2. All samples were cultured for another 4 hr. Dead cells were removed. Samples were pelleted at 4000 rpm for 5 min. All collection procedures were conducted at 4 °C. Cell numbers in each sample were determined. Metabolism was quenched and metabolites were extracted by adding 1 ml −80 °C 80:20 methanol: water per million cells. After 20 min of incubation on dry ice, samples were centrifuged at 10000 g for 5 min. Insoluble pellets were re-extracted with 0.5 ml −80 °C 80: 20 methanol: water on dry ice. The supernatants from two rounds of extraction were combined, dried under N_2, resuspended in 100 μl water per million cells. Metabolites were normalized to cell numbers.

Isotope labeling *in vivo*—Tumor-bearing mice were fasted for 16 hr. $^{13}C_6$-Glc (Cambridge Isotope laboratories) diluted in PBS was given i.p. to mice at 2 g/kg. Spleens and tumors were collected 30 min later. $^{13}C_{16}$-potassium palmitate (Sigma-Aldrich) was conjugated to FA-free BSA (6:1 molar ratio) and given to mice at ~0.35 g/kg by oral gavage. 1 hour later $^{13}C_{16}$-palmitate-BSA was given i.v. at 125 mg/kg. Spleens and tumors were collected 30 min later and cells were isolated on ice. To assess the potential effects of sample processing on lymphocyte metabolism, lymph nodes (LN) were snap frozen on dry ice

immediately upon isolation. In the same experiments, single cell suspensions were prepared from other LNs of the same mice and incubated at 4 °C for 2–2.5 hr prior to the metabolic analyses. $CD44^+CD8^+$ T cells from pooled spleen or tumor samples were stained and sorted at 4 °C. Metabolites were extracted with −80 °C 80: 20 methanol: water, dried under N_2 and resuspended in water at 100 mg tissue/ml or 10^6 cells/100 μl.

LC-MS Instrumentation and method development—Glycolytic and TCA metabolites were analyzed by reversed-phase ion-pairing chromatography coupled with negative-mode electrospray-ionization high-resolution MS on a stand-alone orbitrap (Thermo)(Lu et al., 2010). Carnitine species were analyzed by reversed-phase ion pairing chromatography coupled with positive-mode electrospray-ionization on a Q Exactive hybrid quadrupole-orbitrap mass spectrometer (Thermo); Liquid chromatography separation was achieved on a Poroshell 120 Bonus-RP column (2.1 mm ×150 mm, 2.7 μm particle size, Agilent). The total run time is 25 min, with a flow rate of 50 μl/min from 0 min to 12 min and 200 μl/min from 12 min to 25 min. Solvent A is 98: 2 water: acetonitrile with 10 mM amino acetate and 0.1% acetic acid; solvent B is acetonitrile. The gradient is 0–70% B in 12 min. All isotope-labeling patterns were corrected for natural ^{13}C-abundance.

Electron Microscopy—$CD44^+CD8^+$ T cells were sorted from spleens and TILs of mice bearing day 30 tumors. They were fixed with 2.5% glutaraldehyde, 2.0% paraformaldehyde in 0.1 M sodium cacodylate buffer, pH 7.4, overnight at 4 °C. After washes in buffer, the samples were post-fixed in 2.0% osmium tetroxide for 1 hour at room temperature (RT), and then washed again in buffer followed by distilled H_2O. After dehydration through a graded ethanol series, the samples were infiltrated and embedded in EMbed-812 (Electron Microscopy Sciences). Thin sections were stained with lead citrate and examined with a JEOL 1010 electron microscope fitted with a Hamamatsu digital camera and AMT Advantage image capture software.

Gene expression analysis—Lymphocytes were isolated from spleens and tumors of mice at different time points and stained with dyes and Ab to live cells, $CD8^+$, $CD44^+$ and the Trp-1 and E7 tetramers. For co-adoptive transfer experiments, $CD44^+$ $CD8^+$ T donor cells of different origins were recovered from spleens and tumors of recipient mice upon Ab staining and sorting. Cells were sorted (Mono Astrios, Beckman Coulter) on ice for MAA- or E7-$tet^+CD44^+CD8^+$ T cells into RLT lysis buffer (QIAGEN). For *in vitro* culture samples ~ 10^6 cells/sample were processed on ice to remove dead cells. For lentivector-mediated gene knockdown assays, transduced cells were further purified based on the selection marker using microbeads or cell sorting. RNA was isolated from purified cells using RNeasy Mini kits (Qiagen) and RNA concentrations were determined using Nanodrop (Thermo Scientific). cDNAs were obtained by reverse transcription using the high capacity cDNA reverse transcription kit (Life Technologies). Relative qRT-PCR analyses were performed using 7500 Fast Real-Time PCR system (Life Technologies). β-2 microglobulin or GAPDH were used as internal controls. Vector NTI was used for primers design (Table S1). Differences in transcript expression levels are visualized in heatmaps. Values were log transformed to show ratios of differences. Color scale was set as −2 (lower expression, deep blue) to 2 (higher expression, deep red).

QUANTIFICATION AND STATISTICAL ANALYSIS

All statistical analyses were conducted using GraphPad Prism 6 (GraphPad). Differences between 2 populations were calculated by Student's t-test. Multiple comparisons between two groups were performed by multiple t-test with type I error correction. Differences among multiple populations were calculated by one- or two-way ANOVA. Differences in survival were calculated by Log-rank Mantel-Cox test. Differences between tumor growth curves were determined by repeated measures two-way ANOVA. Type I errors were corrected by Holm-Šídák method. Significance was set at p values of or below 0.05. For all figures, *p ≤0.05 – 0.01, ** p≤0.01–0.001, *** p ≤0.001–0.0001, **** p≤0.0001. Unless noted in the figure legend, all data are shown as mean +/− SEM. The n numbers for each experiment, as well as the numbers of experiments that has been repeated have been noted in the figure legends.

Supplementary Material

Refer to Web version on PubMed Central for supplementary material.

Acknowledgments

We thank the NIH Tetramer Core Facility for tetramers; J. Faust, Y. Li, Drs. Z.Q. Xiang, A. Kossenkov, Y. Nefedova (Wistar Institute), R. Meade, X. Zuo and Dr. K. Foskett (U of PA) for help with reagents and equipment; Dr. Z. Schug for discussions and Drs. P. Matzinger and Y. Paterson for reviewing the manuscript. Funding: Wistar Vaccine Center Funding; NCI grants CA114046, CA174523, P50CA101942; DoD PRCRP CA1150619 and Dr. Miriam and Sheldon G. Adelson Medical Research Foundation.

References

Azuma T, Yao S, Zhu G, Flies AS, Flies SJ, Chen L. B7-H1 is a ubiquitous antiapoptotic receptor on cancer cells. Blood. 2008; 111:3635–3643. DOI: 10.1182/blood-2007-11-123141 [PubMed: 18223165]

Balmer ML, Ma EH, Bantug GR, Grählert J, Pfister S, Glatter T, Jauch A, Dimeloe S, Slack E, Dehio P, Krzyzaniak MA, King CG, Burgener AV, Fischer M, Develioglu L, Belle R, Recher M, Bonilla WV, Macpherson AJ, Hapfelmeier S, Jones RG, Hess C. Memory CD8+ T Cells Require Increased Concentrations of Acetate Induced by Stress for Optimal Function. Immunity. 2016; 44:1312–1324. DOI: 10.1016/j.immuni.2016.03.016 [PubMed: 27212436]

Bucks CM, Norton JA, Boesteanu AC, Mueller YM, Katsikis PD. Chronic antigen stimulation alone is sufficient to drive CD8+ T cell exhaustion. J Immunol. 2009; 182:6697–6708. DOI: 10.4049/jimmunol.0800997 [PubMed: 19454664]

Chamoto K, Chowdhury PS, Kumar A, Sonomura K, Matsuda F, Fagarasan S, Honjo T. Mitochondrial activation chemicals synergize with surface receptor PD-1 blockade for T cell-dependent antitumor activity. Proceedings of the National Academy of Sciences. 2017; 114:E761–E770. DOI: 10.1073/pnas.1620433114

Chang C-H, Qiu J, O'Sullivan D, Buck MD, Noguchi T, Curtis JD, Chen Q, Gindin M, Gubin MM, van der Windt GJW, Tonc E, Schreiber RD, Pearce EJ, Pearce EL. Metabolic Competition in the Tumor Microenvironment Is a Driver of Cancer Progression. Cell. 2015; :1–14. DOI: 10.1016/j.cell.2015.08.016

Chen L, Han X. Anti-PD-1/PD-L1 therapy of human cancer: past, present, and future. J Clin Invest. 2015; 125:3384–3391. DOI: 10.1172/JCI80011 [PubMed: 26325035]

Crompton JG, Sukumar M, Roychoudhuri R, Clever D, Gros A, Eil RL, Tran E, Hanada KI, Yu Z, Palmer DC, Kerkar SP, Michalek RD, Upham T, Leonardi A, Acquavella N, Wang E, Marincola FM, Gattinoni L, Muranski P, Sundrud MS, Klebanoff CA, Rosenberg SA, Fearon DT, Restifo NP. Akt Inhibition Enhances Expansion of Potent Tumor-Specific Lymphocytes with Memory Cell

Characteristics. Cancer Res. 2015; 75:296–305. DOI: 10.1158/0008-5472.CAN-14-2277 [PubMed: 25432172]

Dalgleish AG. Therapeutic cancer vaccines: Why so few randomised phase III studies reflect the initial optimism of phase II studies. Vaccine. 2011; 29:8501–8505. DOI: 10.1016/j.vaccine.2011.09.012 [PubMed: 21933695]

Doedens AL, Phan AT, Stradner MH, Fujimoto JK, Nguyen JV, Yang E, Johnson RS, Goldrath AW. Hypoxia-inducible factors enhance the effector responses of CD8+ T cells to persistent antigen. Nat Immunol. 2013; 14:1173–1182. DOI: 10.1038/ni.2714 [PubMed: 24076634]

Finlay DK, Rosenzweig E, Sinclair LV, Feijoo-Carnero C, Hukelmann JL, Rolf J, Panteleyev AA, Okkenhaug K, Cantrell DA. PDK1 regulation of mTOR and hypoxia-inducible factor 1 integrate metabolism and migration of CD8+ T cells. J Cell Biol. 2012; 199:i8–i8. DOI: 10.1083/JCB1996OIA8

Grosso JF, Kelleher CC, Harris TJ, Maris CH, Hipkiss EL, De Marzo A, Anders R, Netto G, Getnet D, Bruno TC, Goldberg MV, Pardoll DM, Drake CG. LAG-3 regulates CD8+ T cell accumulation and effector function in murine self- and tumor-tolerance systems. J Clin Invest. 2007; 117:3383–3392. DOI: 10.1172/JCI31184 [PubMed: 17932562]

Hamanaka RB, Chandel NS. Targeting glucose metabolism for cancer therapy. Journal of Experimental Medicine. 2012; 209:211–215. DOI: 10.1084/jem.20120162 [PubMed: 22330683]

Hamid O, Robert C, Daud A, Hodi FS, Hwu WJ, Kefford R, Wolchok JD, Hersey P, Joseph RW, Weber JS, Dronca R, Gangadhar TC, Patnaik A, Zarour H, Joshua AM, Gergich K, Elassaiss-Schaap J, Algazi A, Mateus C, Boasberg P, Tumeh PC, Chmielowski B, Ebbinghaus SW, Li XN, Kang SP, Ribas A. Safety and tumor responses with lambrolizumab (anti-PD-1) in melanoma. N Engl J Med. 2013; 369:134–144. DOI: 10.1056/NEJMoa1305133 [PubMed: 23724846]

Ho PC, Bihuniak JD, Macintyre AN, Staron M, Liu X, Amezquita R, Tsui YC, Cui G, Micevic G, Perales JC, Kleinstein SH, Abel ED, Insogna KL, Feske S, Locasale JW, Bosenberg MW, Rathmell JC, Kaech SM. Phosphoenolpyruvate Is a Metabolic Checkpoint of Anti-tumor T Cell Responses. Cell. 2015; 162:1217–1228. DOI: 10.1016/j.cell.2015.08.012 [PubMed: 26321681]

Kaech SM, Cui W. Transcriptional control of effector and memory CD8+ T cell differentiation. Nature Reviews Immunology. 2012; 12:749–761. DOI: 10.1038/nri3307

Larkin J, Chiarion-Sileni V, Gonzalez R, Grob JJ, Cowey CL, Lao CD, Schadendorf D, Dummer R, Smylie M, Rutkowski P, Ferrucci PF, Hill A, Wagstaff J, Carlino MS, Haanen JB, Maio M, Marquez-Rodas I, McArthur GA, Ascierto PA, Long GV, Callahan MK, Postow MA, Grossmann K, Sznol M, Dréno B, Bastholt L, Yang A, Rollin LM, Horak C, Hodi FS, Wolchok JD. Combined Nivolumab and Ipilimumab or Monotherapy in Untreated Melanoma. N Engl J Med. 2015; 373:23–34. DOI: 10.1056/NEJMoa1504030 [PubMed: 26027431]

Lasaro MO, Tatsis N, Hensley SE, Whitbeck JC, Lin SW, Rux JJ, Wherry EJ, Cohen GH, Eisenberg RJ, Ertl HC. Targeting of antigen to the herpesvirus entry mediator augments primary adaptive immune responses. Nat Med. 2008; 14:205–212. DOI: 10.1038/nm1704 [PubMed: 18193057]

Lu W, Clasquin MF, Melamud E, Amador-Noguez D, Caudy AA, Rabinowitz JD. Metabolomic analysis via reversed-phase ion-pairing liquid chromatography coupled to a stand alone orbitrap mass spectrometer. Anal Chem. 2010; 82:3212–3221. DOI: 10.1021/ac902837x [PubMed: 20349993]

Martinez-Outschoorn UE, Lin Z, Whitaker-Menezes D, Howell A, Sotgia F, Lisanti MP. Ketone body utilization drives tumor growth and metastasis. Cell Cycle. 2012; 11:3964–3971. DOI: 10.4161/cc.22137 [PubMed: 23082722]

McNamee EN, Korns Johnson D, Homann D, Clambey ET. Hypoxia and hypoxia-inducible factors as regulators of T cell development, differentiation, and function. Immunol Res. 2013; 55:58–70. DOI: 10.1007/s12026-012-8349-8 [PubMed: 22961658]

Menendez JA, Lupu R. Fatty acid synthase and the lipogenic phenotype in cancer pathogenesis. Nat Rev Cancer. 2007; 7:763–777. DOI: 10.1038/nrc2222 [PubMed: 17882277]

Mrass P, Takano H, Ng LG, Daxini S, Lasaro MO, Iparraguirre A, Cavanagh LL, von Andrian UH, Ertl HCJ, Haydon PG, Weninger W. Random migration precedes stable target cell interactions of tumor-infiltrating T cells. Journal of Experimental Medicine. 2006; 203:2749–2761. DOI: 10.1084/jem.20060710 [PubMed: 17116735]

Mueller SN, Ahmed R. High antigen levels are the cause of T cell exhaustion during chronic viral infection. Proc Natl Acad Sci USA. 2009; 106:8623–8628. DOI: 10.1073/pnas.0809818106 [PubMed: 19433785]

O'Sullivan D, van der Windt GJW, Huang SCC, Curtis JD, Chang CH, Buck MD, Qiu J, Smith AM, Lam WY, DiPlato LM, Hsu FF, Birnbaum MJ, Pearce EJ, Pearce EL. Memory CD8(+) T cells use cell-intrinsic lipolysis to support the metabolic programming necessary for development. Immunity. 2014; 41:75–88. DOI: 10.1016/j.immuni.2014.06.005 [PubMed: 25001241]

Ohta A, Diwanji R, Kini R, Subramanian M, Ohta A, Sitkovsky M. In vivo T cell activation in lymphoid tissues is inhibited in the oxygen-poor microenvironment. Front Immunol. 2011; 2:27.doi: 10.3389/fimmu.2011.00027 [PubMed: 22566817]

Parry RV, Chemnitz JM, Frauwirth KA, Lanfranco AR, Braunstein I, Kobayashi SV, Linsley PS, Thompson CB, Riley JL. CTLA-4 and PD-1 Receptors Inhibit T-Cell Activation by Distinct Mechanisms. Mol Cell Biol. 2005; 25:9543–9553. DOI: 10.1128/MCB.25.21.9543-9553.2005 [PubMed: 16227604]

Patsoukis N, Bardhan K, Chatterjee P, Sari D, Liu B, Bell LN, Karoly ED, Freeman GJ, Petkova V, Seth P, Li L, Boussiotis VA. PD-1 alters T-cell metabolic reprogramming by inhibiting glycolysis and promoting lipolysis and fatty acid oxidation. Nature Communications. 2015; 6:6692.doi: 10.1038/ncomms7692

Patsoukis N, Li L, Sari D, Petkova V, Boussiotis VA. PD-1 increases PTEN phosphatase activity while decreasing PTEN protein stability by inhibiting casein kinase 2. Mol Cell Biol. 2013; 33:3091–3098. DOI: 10.1128/MCB.00319-13 [PubMed: 23732914]

Siska PJ, Beckermann KE, Mason FM, Andrejeva G, Greenplate AR, Sendor AB, Chiang YCJ, Corona AL, Gemta LF, Vincent BG, Wang RC, Kim B, Hong J, Chen CL, Bullock TN, Irish JM, Rathmell WK, Rathmell JC. Mitochondrial dysregulation and glycolytic insufficiency functionally impair CD8 T cells infiltrating human renal cell carcinoma. JCI Insight. 2017; 2:1–13. DOI: 10.1172/jci.insight.93411

Sukumar M, Liu J, Ji Y, Subramanian M, Crompton JG, Yu Z, Roychoudhuri R, Palmer DC, Muranski P, Karoly ED, Mohney RP, Klebanoff CA, Lal A, Finkel T, Restifo NP, Gattinoni L. Inhibiting glycolytic metabolism enhances CD8+ T cell memory and antitumor function. J Clin Invest. 2013; 123:4479–4488. DOI: 10.1172/JCI69589 [PubMed: 24091329]

Takahashi S, Iizumi T, Mashima K, Abe T, Suzuki N. Roles and regulation of ketogenesis in cultured astroglia and neurons under hypoxia and hypoglycemia. ASN Neuro. 2014; 6:1759091414550997.doi: 10.1177/1759091414550997 [PubMed: 25290061]

Tatsis N, Fitzgerald JC, Reyes-Sandoval A, Harris-McCoy KC, Hensley SE, Zhou D, Lin SW, Bian A, Xiang ZQ, Iparraguirre A, Lopez-Camacho C, Wherry EJ, Ertl HCJ. Adenoviral vectors persist in vivo and maintain activated CD8+ T cells: implications for their use as vaccines. Blood. 2007; 110:1916–1923. DOI: 10.1182/blood-2007-02-062117 [PubMed: 17510320]

Veech RL. The therapeutic implications of ketone bodies: the effects of ketone bodies in pathological conditions: ketosis, ketogenic diet, redox states, insulin resistance, and mitochondrial metabolism. Prostaglandins Leukot Essent Fatty Acids. 2004; 70:309–319. DOI: 10.1016/j.plefa.2003.09.007 [PubMed: 14769489]

Wiig H, Aukland K, Tenstad O. Isolation of interstitial fluid from rat mammary tumors by a centrifugation method. Am J Physiol Heart Circ Physiol. 2003; 284:H416–24. DOI: 10.1152/ajpheart.00327.2002 [PubMed: 12388326]

Zhang Y, Ertl HCJ. The effect of adjuvanting cancer vaccines with herpes simplex virus glycoprotein D on melanoma-driven CD8+ T cell exhaustion. J Immunol. 2014; 193:1836–1846. DOI: 10.4049/jimmunol.1302029 [PubMed: 25024391]

Zhu Y, Ju S, Chen E, Dai S, Li C, Morel P, Liu L, Zhang X, Lu B. T-bet and eomesodermin are required for T cell-mediated antitumor immune responses. J Immunol. 2010; 185:3174–3183. DOI: 10.4049/jimmunol.1000749 [PubMed: 20713880]

Zou W, Wolchok JD, Chen L. PD-L1 (B7-H1) and PD-1 pathway blockade for cancer therapy: Mechanisms, response biomarkers, and combinations. Sci Transl Med. 2016; 8:328rv4–328rv4. DOI: 10.1126/scitranslmed.aad7118

Significance

Metabolic fitness is critical for cell functions. Dysregulated metabolism contributes to the exhaustion of TILs within the TME. If and how TILs adjust their metabolism to maintain functional remains to be explored. We show that hypoxia and hypoglycemia, two major metabolic challenges within the TME, impair $CD8^+$ TILs through distinct pathways. Using two mouse melanoma models and human melanoma samples, our study shows that $CD8^+$ TILs experiencing double metabolic jeopardy enhance PPAR-α signaling and fatty acid (FA) catabolism to preserve energy production and effector functions. Promoting FA catabolism with fenofibrate markedly improves their capacity to delay tumor growth. It synergizes with PD-1 blockade to efficiently boost the efficacy of melanoma immunotherapy.

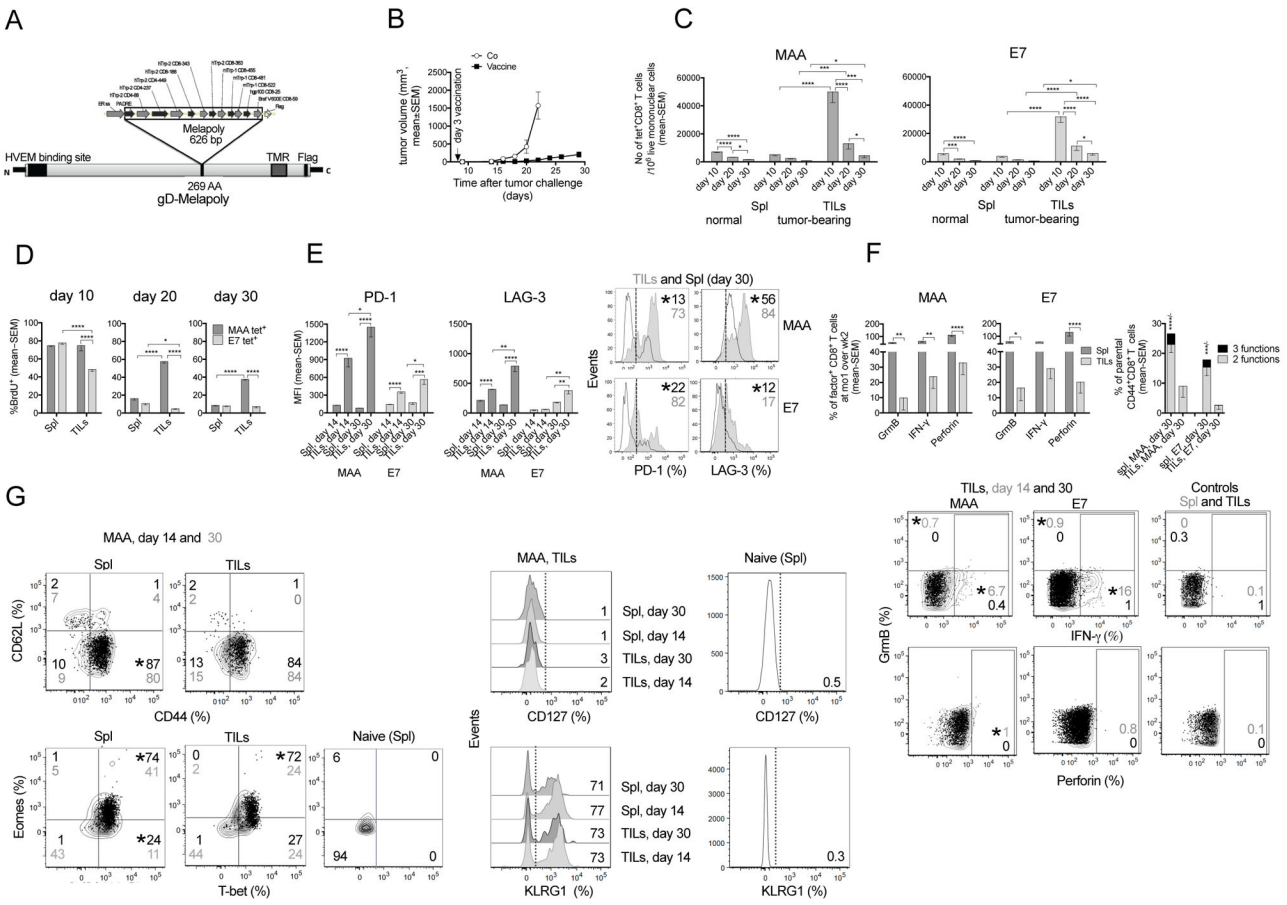

Fig 1. CD8$^+$ TILs become functionally impaired

(A) AdC68-gDMelapoly transgene. (B) B16Braf$_{V600E}$ tumor growth curves (Co [AdC68-gD], n=6; Vaccine, n=18). (C) Numbers of Trp-1 (MAA)- and E7-tetramer (tet)$^+$CD8$^+$ T cells/10^6 live mononuclear cells in spleens (Spl) and tumors of mice that had or had not been received tumor cells before vaccination (n=10/group). (D) % BrdU incorporation into antigen-specific CD8$^+$ T cells from Spl and tumors. (E) Mean fluorescent intensity (MFI) and histograms for PD-1 and LAG-3 on CD8$^+$ T cells from Spl (open histogram) and tumors (grey histogram) at 14 or 30 days after tumor challenge. (F) Left: Relative % antigen-specific CD8$^+$ T cells from Spl and tumors producing GrmB, perforin or IFN-γ comparing day 30 to 14 samples. Right: % specific CD8$^+$ T cells at day 30 from Spl or tumors producing 3 or 2 of the tested functions. The same functions are displayed throughout the manuscript unless indicated otherwise. * bottom to top: significant differences in 2 and 3 functions. Bottom: flow plot showing TIL functions: day 14 (grey) vs. 30 (black) overlays; control: Spl and TILs stimulated with irrelevant peptide. (G) Differentiation markers on MAA-specific T cells from Spl and tumors: as day 14 (black) vs. 30 (grey) overlays (left) or histograms (right). Gating control: Naive CD8$^+$ T cells. (E–G) Numbers in plots: average % marker$^+$ cells for the entire group; stars next to top number indicate significant differences between groups. This applies to all flow plots in the manuscript. (D–G) n=5/group. Data show mean with SEM. Data represent 2 (B, D, F, G) or 3 assays (C, E). For all figures, *p ≤0.05 – 0.01, ** p≤0.01–0.001, *** p ≤0.001–0.0001, **** p≤0.0001. See also Figure S1.

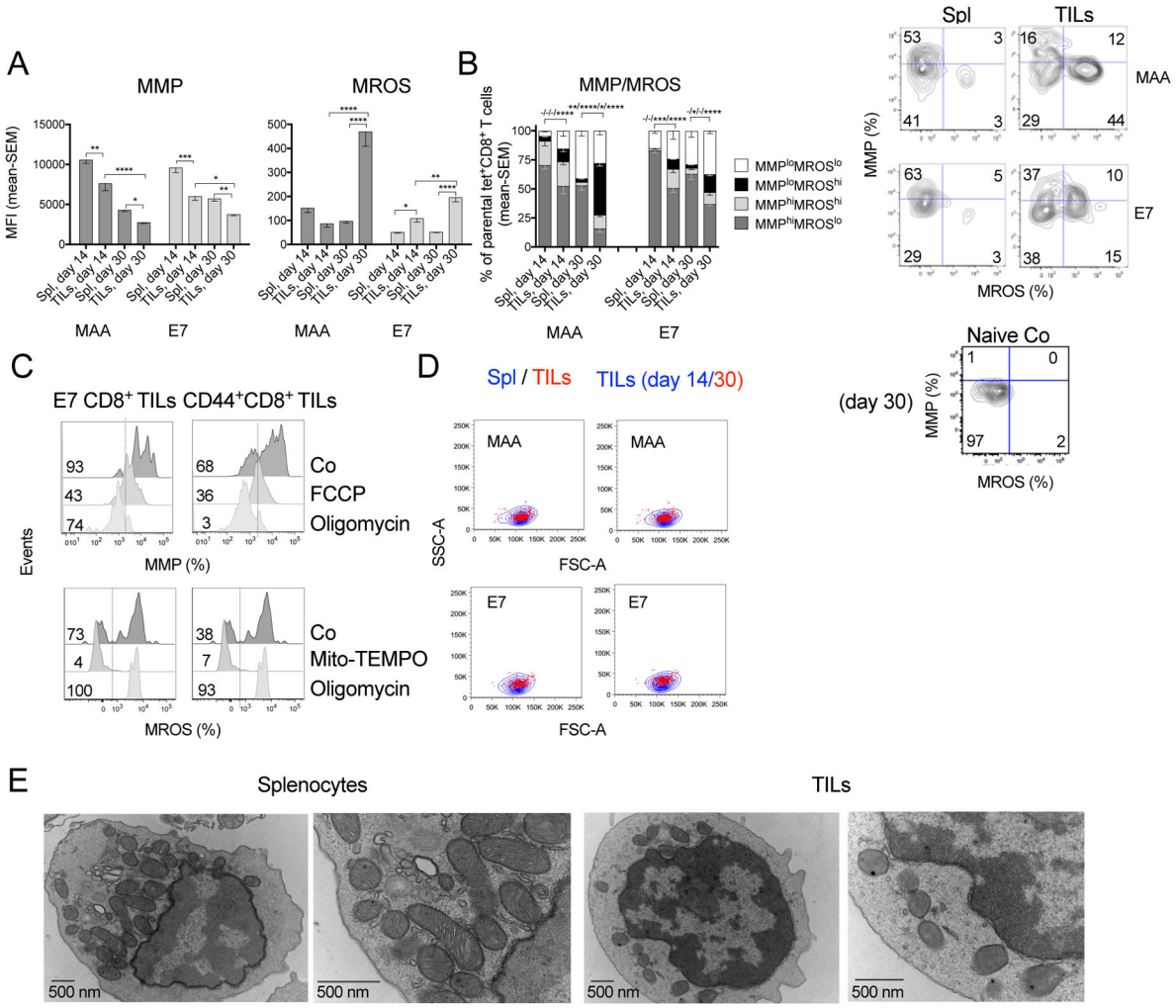

Figure 2. CD8$^+$ TILs increasingly experience metabolic stress

(A) MFI of MMP and MROS in specific CD8$^+$ T cells from Spl and tumors. (B) Left: MMP over MROS of CD8$^+$ T cells from Spl and tumors. (−) not significant or (*) significant differences left to right are for populations from top to bottom in legend. Right: flow plots of specific T cells from day 30 tissues and naive T cells (Co). (C) Controls for DioC6 and Mitosox Red stains on CD8$^+$ TILs. CD44$^+$CD8$^+$ TILs and E7-specific CD8$^+$ TILs were treated with FCCP or oligomycin to collapse the MMP; with Mito-TEMPO to reduce MROS, or with oligomycin to induce MROS. (D) MAA- or E7-specific CD8$^+$ T cell size comparison between those from Spl and tumors isolated from mice bearing day 14 or 30 tumors. Representative flow plots show cell subsets overlay upon gating on FSC over SSC. (E) Transmission electron micrographs of CD44$^+$CD8$^+$ T cells from day 30 Spl and tumors. Samples pooled from 15 mice. Data show mean - SEM; representative of 3 (A–C) or 2 assays (D).

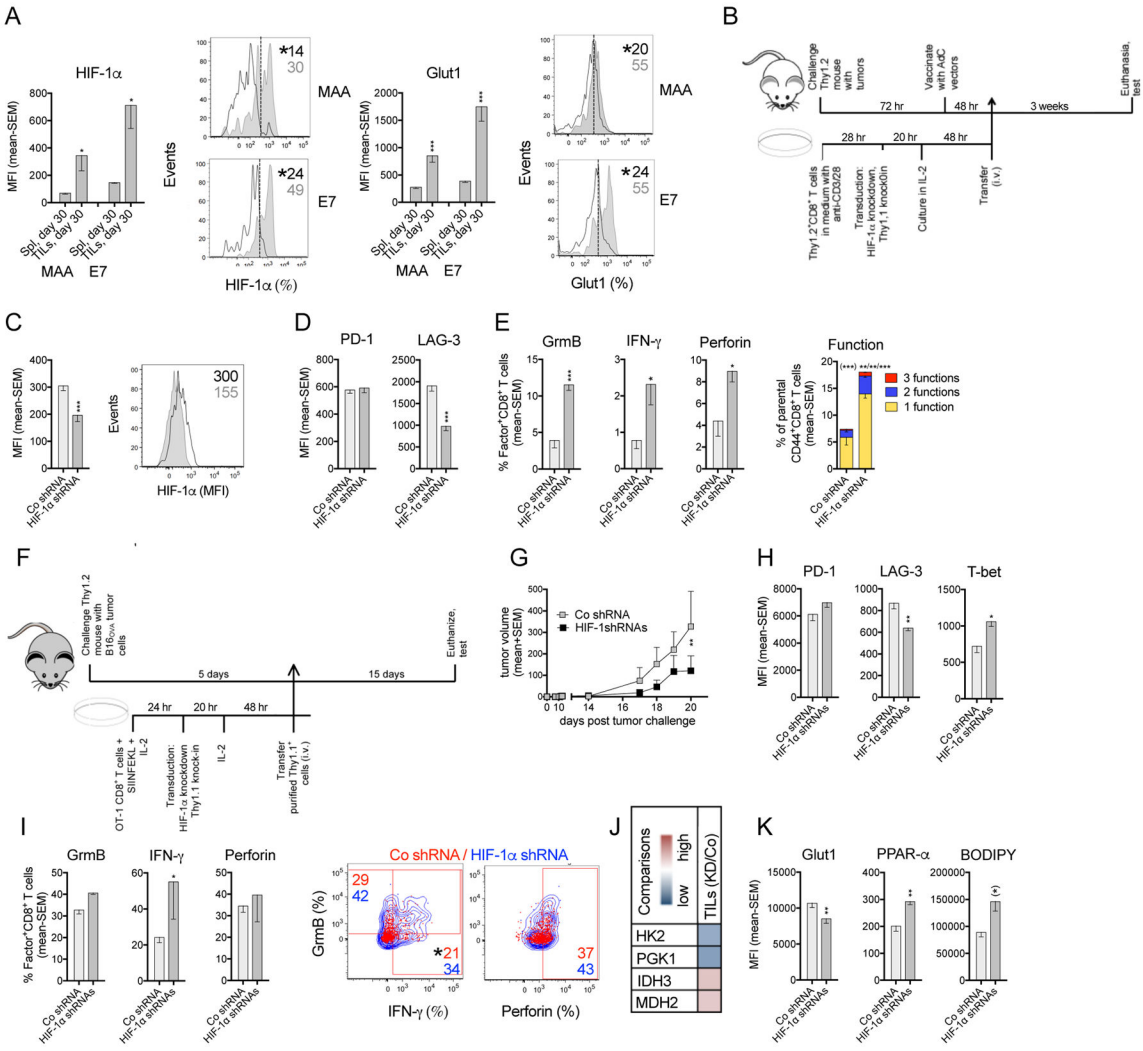

Figure 3. Effect of HIF-1α knockdown on TA-specific CD8$^+$ TILs

(A) MFI and representative histograms of HIF-1α and Glut1 in/on specific CD8$^+$ T cells from day 30 Spl (open) and tumors (grey) (n=5 mice/group). (B) Experimental set-up: vaccine model. (C) MFI and flow plot of HIF-1α in MAA-specific CD8$^+$ TILs transduced with scrambled (Co, open histogram) or HIF-1α shRNA lentivector (grey histogram). (D) MFI of PD-1 and LAG-3. (E) Left: % transduced MAA-specific CD8$^+$ TILs producing individual functions. Right: Polyfunctionality. % transduced cells producing 3, 2 or 1 of the 3 tested functions. For all figures: * within (): significant difference in sum of responses. * without () left to right: significant difference in 3, 2, and 1 functions. (C–E) n=5–7 mice/group. (F) Experimental set up: OT-1 transfer model. (G) Tumor growth in mice that received transduced OT-1 T cells. (H) MFI of PD-1, LAG-3 and T-bet on/in donor transduced OT-1 CD8$^+$ TILs. (I) Left: % transduced donor OT-1 CD8$^+$ TILs producing individual factors. Right: flow plots show overlays of HIF-1α shRNA (blue) and Co (red) transduced factor-producing OT-1 CD8$^+$ TILs. (J) Heatmap of transcript levels comparing HIF-1α shRNA over Co transduced OT-1 CD8$^+$ TILs. (K) MFI of Glut1, PPAR-α and

BODIPY C_{16} uptake. (*): p=0.05. (G–K) n=5–8 mice/group. Experiments were repeated twice. Data show mean - SEM. See also Figures S2, S3.

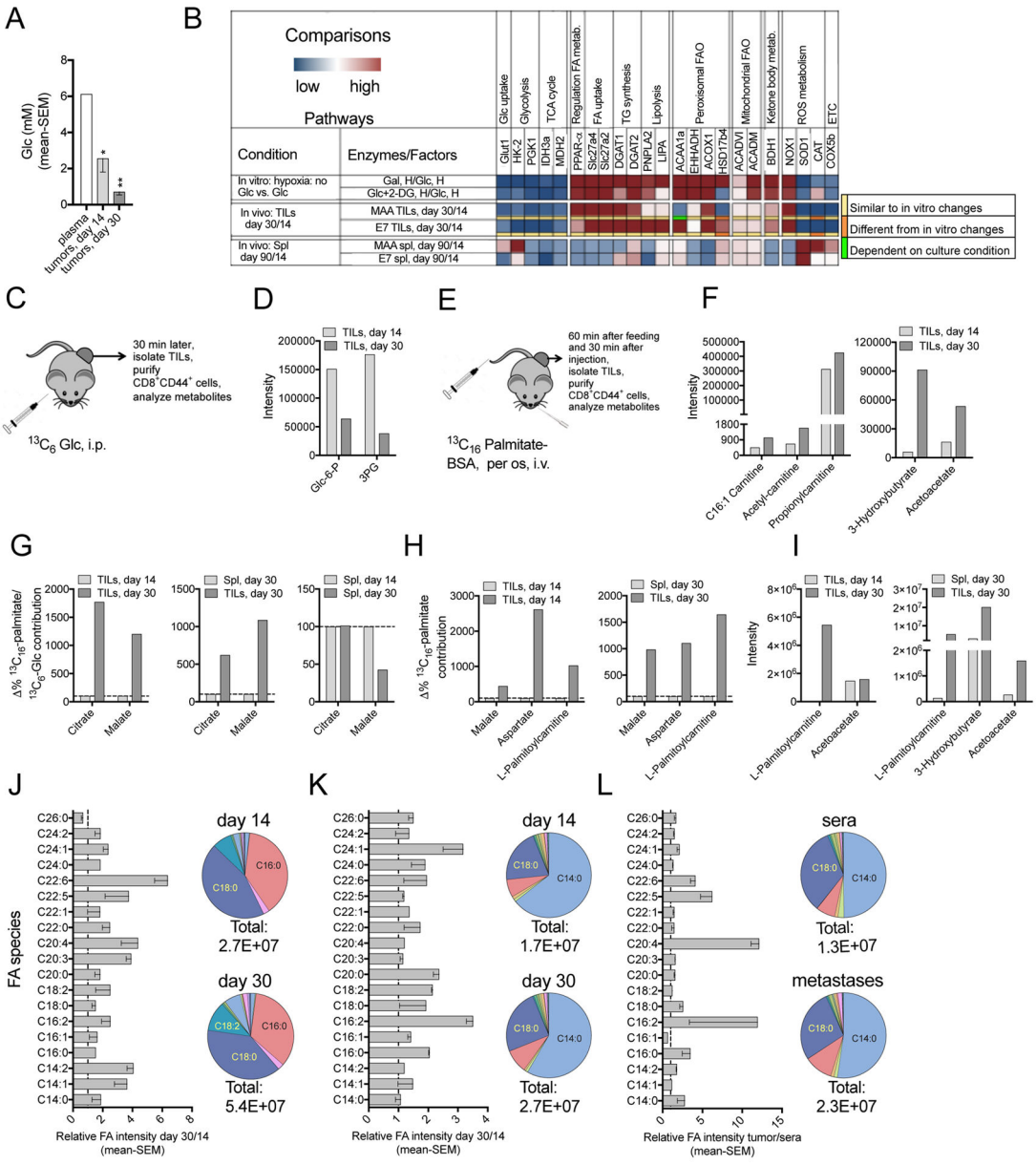

Figure 4. Limited access to Glc and O_2 forces $CD8^+$ TILs to enhance FA catabolism

(A–G) Vaccine model. (A) Glc concentrations in plasma, early and late stage $B16Braf_{V600E}$ tumors (n=3). (B) Relative transcript levels: Upper: $CD8^+$ T cells in Gal- or Glc+2-DG- vs. Glc-medium under hypoxia. Middle: specific $CD8^+$ TILs from day 30 vs. 14 tumors. Lower: specific $CD8^+$ T harvested from day 90 vs. 14 Spl (n=3). Color code below 3rd and 4th row: comparisons between *in vitro* and *in vivo* samples. (C) Experimental set-up: $^{13}C_6$-Glc *in vivo* tracing. (D) Intensity of glycolysis metabolites in $CD44^+CD8^+$ TILs. (E) Experimental set-up: $^{13}C_{16}$-palmitate *in vivo* tracing. (F) Intensity of FA metabolites in $CD44^+CD8^+$ TILs. (G) Relative contribution of $^{13}C_6$-Glc- and $^{13}C_{16}$- palmitate-derived carbons to citrate and malate, calculated by dividing labeling carbon numbers from $^{13}C_{16}$-palmitate by the numbers from $^{13}C_6$-Glc. Data of $CD44^+CD8^+$ T cells from day 30 tumors are normalized to

those from day 14 tumors (left) or day 30 Spl (middle); Spl data: day 30 normalized to 14 (right). (D, F, G) n=2–3, pooled from ~30 mice/sample. (H–I) OT-1 transfer model. (H) Normalized contribution of $^{13}C_{16}$-palmitate to TCA cycle metabolites and L-palmitoylcarnitine in $CD44^{+}CD8^{+}$ TILs from day 30 vs. 14 tumors or day 30 Spl. (I) Intensities of FA metabolites. (H–I) n=2, pooled from ~20 mice/sample. (D, F, G–I) Data show as mean values. (J–L) Bar graphs: Relative intensity of free FA species in tumor interstitial fluid, dashed lines show ratio of 1. Pie charts: Abundance of different FA species. Total numbers: combined FA intensity. (J–K) day 30 over 14 $B16Braf_{V600E}$ tumors (J, n=3) or PDX melanomas (K, n = 5). (L) Human melanoma metastases vs. human sera (n = 4). (D, F, G–L) Representative of two assays. (A, J–L) mean - SEM. See also Figures S4, S5.

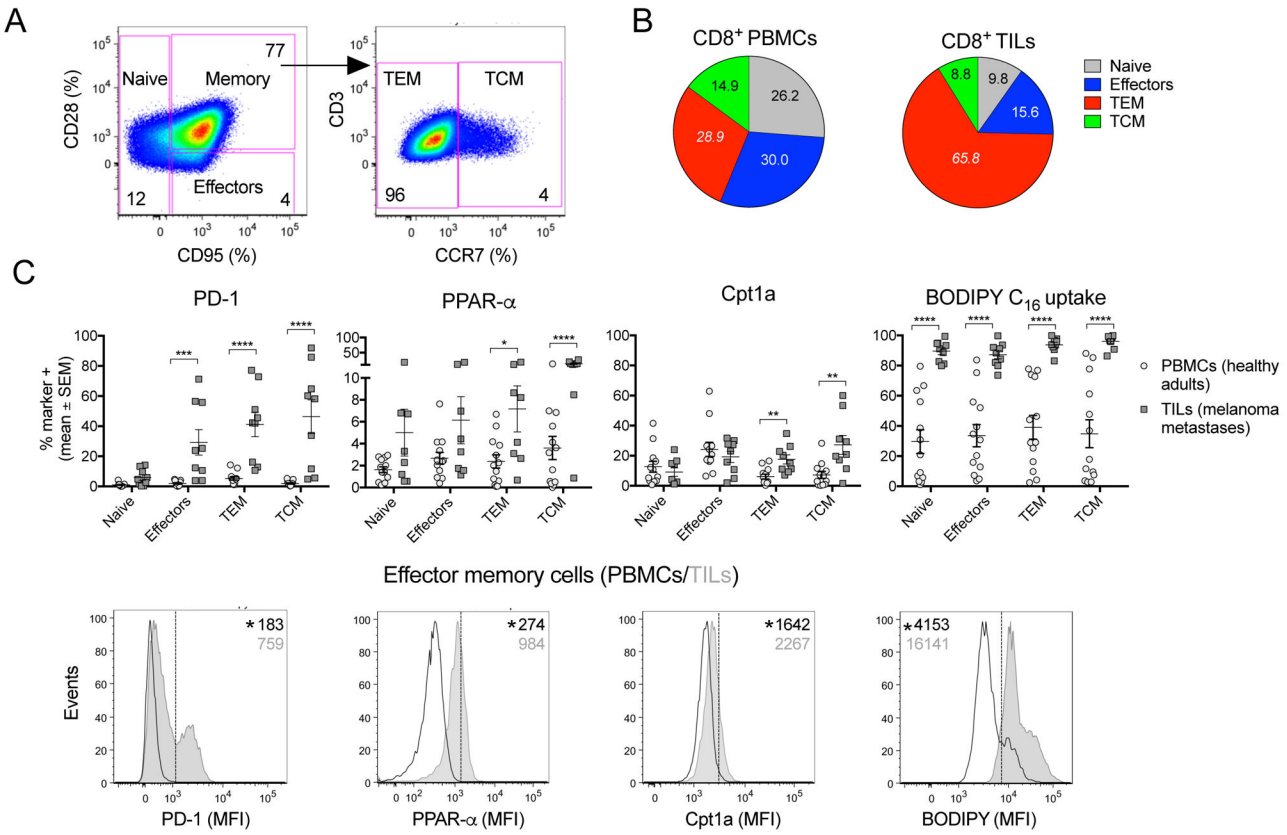

Figure 5. Metabolism of T cells in human samples

(A) Gating strategy for human $CD8^+$ T cells subsets. Numbers show % of cells in each subset. (B) Pie charts show distribution of $CD8^+$ T cell subsets within $CD8^+$ T cells isolated from blood of healthy donors (n=14) or metastatic tumors of melanoma patients (n=9). $p<0.0001$ for differences in numbers of TEM cells normalized to 10^6 live $CD8^+$ T cells. Numbers within pie charts show mean percentages. (C) Upper: % of cells positive for PD-1, Cpt1a, PPAR-α and FA uptake (BODIPY C_{16}). Data show comparison for $CD8^+$ T cell subsets isolated from blood vs. tumors. Lower: Representative histograms comparing markers of $CD8^+$ TEM from blood vs. tumors. Data show mean - SEM.

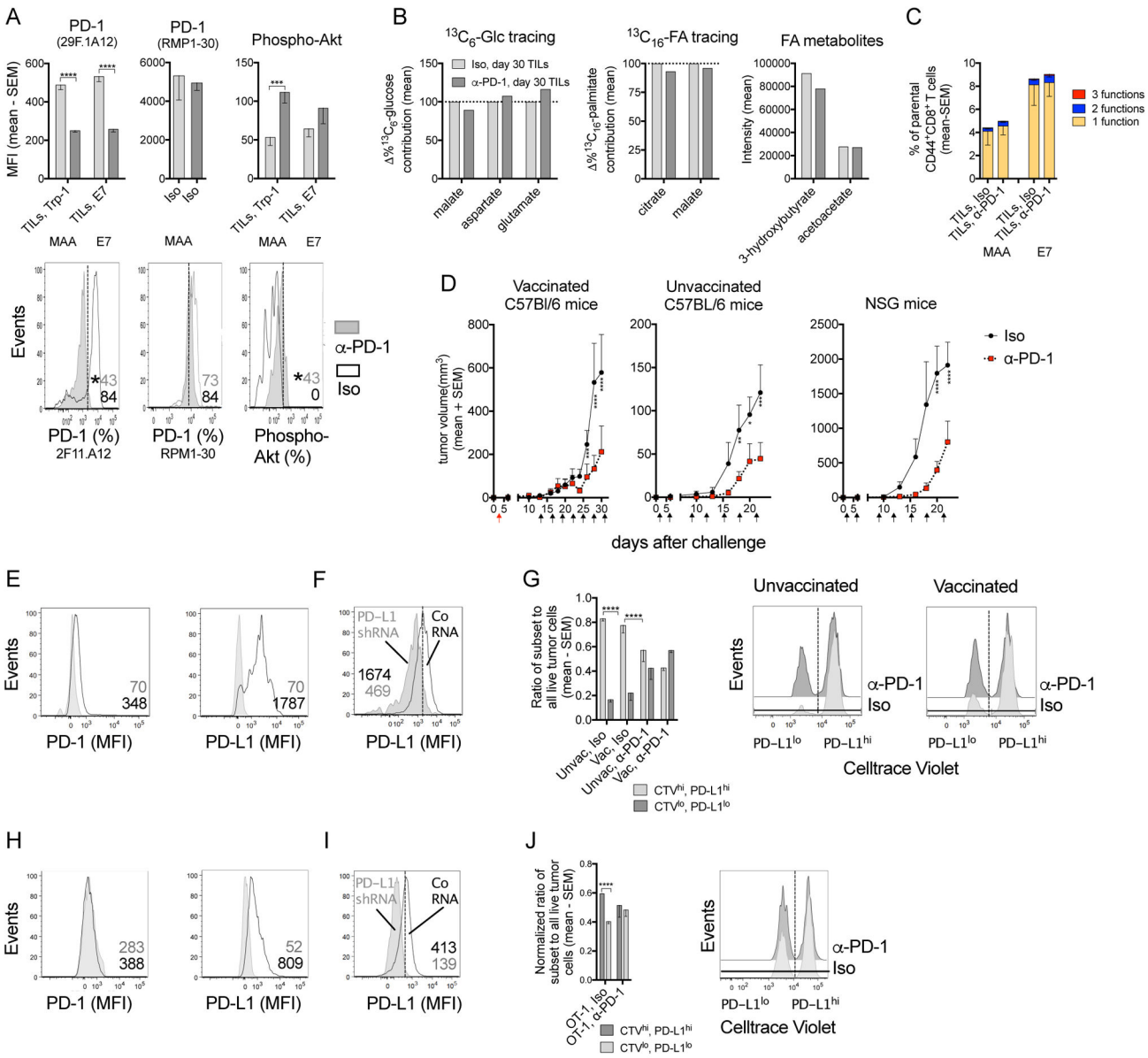

Figure 6. Metabolism and effector functions of CD8$^+$ TILs are independent of PD-1

(A) MFI of PD-1 tested with PD-1 Ab clone 29F.1A12 (same clone as α-PD-1 treatment Ab) or RMP1-30 and Phospho-Akt on/in specific CD8$^+$ TILs from day 30 tumors (n=5–7). Iso: isotype control mAb. Lower: Flow plots for MAA-specific TILs. (B) Normalized $^{13}C_6$-Glc or $^{13}C_{16}$-palmitate contribution to TCA cycle metabolites and the intensity of ketone bodies in CD44$^+$CD8$^+$ T cells from day 30 tumors comparing α-PD-1- to Iso-treated mice. n=2 or 3, pooled from 25 mice/sample, shown as mean values. (C) % specific CD8$^+$ TILs from day 30 tumors producing 3, 2 or 1 of the 3 tested functions (Iso: n=11; α-PD-1: n=15; data pooled from two assays). (D) B16Braf$_{V600E}$ tumor growth in mice that received Iso or α-PD-1 (unvaccinated: n=5; vaccinated: n=13; NSG: n=4). Arrows: red (vaccine); black (Ab treatment). (E) PD-1 and PD-L1 on B16Braf$_{V600E}$ tumor cells grown *in vivo*. Iso (grey), specific Ab (open). (F) PD-L1 KD in B16Braf$_{V600E}$ cells. (G) *In vivo* assay comparing

survival of PD-L1^{hi}CTV^{hi} vs. PD-L1^{lo}CTV^{lo} tumor cells in vaccinated or unvaccinated mice treated with Iso or α-PD-1 mAb. Bar graph: ratio of recovered live PD-L1^{hi} over PD-L1^{lo} B16Braf$_{V600E}$ cells (n=5). Right: histograms. (H) PD-1 and PD-L1 on B16$_{OVA}$ tumor cells grown *in vivo*. (I) PD-L1 KD in B16$_{OVA}$ cells. (J) Normalized survival of PD-L1^{hi}CTV^{hi} vs. PD-L1^{lo}CTV^{lo} B16$_{OVA}$ cells in Iso or α-PD-1-treated mice that were transferred with activated OT-1 cells and representative histograms (n=5). (A, C, D, G, J) Data show mean with SEM (representative of 2 experiments). See also Figures S6.

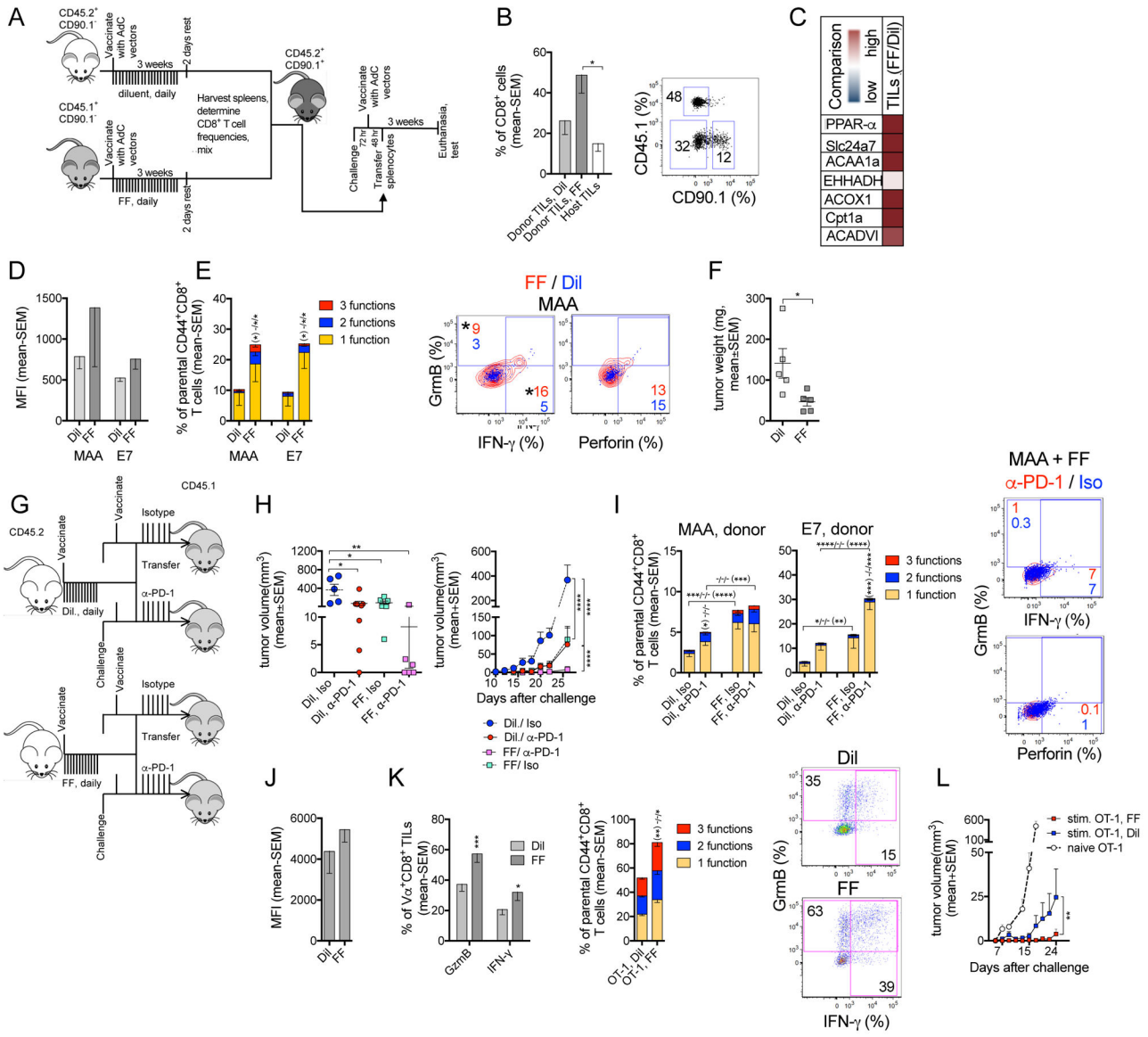

Figure 7. Promoting FA catabolism improves CD8$^+$ TIL functions and works in synergy with PD-1 blockade to delay tumor growth

(A–F) Vaccine model. (A) Experimental design. (B) % donor and host CD8$^+$ T cells from tumors of recipients as bar graphs (left) or flow plot (right). (C) Transcript levels in donor-derived FF-vs. Dil-treated CD44$^+$CD8$^+$ TILs (n=3–4/group). (D) MFIs of PD-1 on specific donor CD8$^+$ TILs. (E) Left: % specific donor CD8$^+$ TILs producing 3, 2, or 1 of the 3 tested functions; * from bottom to top: differences in 3-1 factors; Right: Representative plots overlays of FF- (red) and Dil- (blue) treated MAA-specific donor TILs. (F) B16Braf$_{V600E}$ tumor weight at necropsy. (D–F, n=5). (G–I) PD-1 blockade combined with FF treatment. (G) Experimental design. (H) Left: tumor volume at day 30; Right: tumor growth curves. (I) Functions of donor CD8$^+$ TILs. * bottom to top or right to left: differences cells producing 3, 2, or 1 of the 3 tested functions. Flow plots: factor-producing MAA-specific TILs from mice that received FF-treated cells, α-PD-1 (red) overlaid with Iso (blue)-treated cells. (H, I)

Iso: n=6; α-PD-1: n=7. Studies were repeated twice. (J–L) OT-1 transfer model. (J) MFI of PD-1 on FF- or Dil-treated donor-derived activated OT-1 TILs. (K) Left: % donor-derived OT-1 TILs producing GrmB or IFN-γ. Middle: % cells producing 3, 2, or 1 of the 3 tested functions. Right: flow plots. (J, K) n=8 mice/group; data represent 2 experiments. (L) $B16_{OVA}$ tumor growth in mice received naive (n=24), Dil- or FF-treated activated OT-1 T cells (n=8/group). Data show mean - SEM. See also Figure S7.

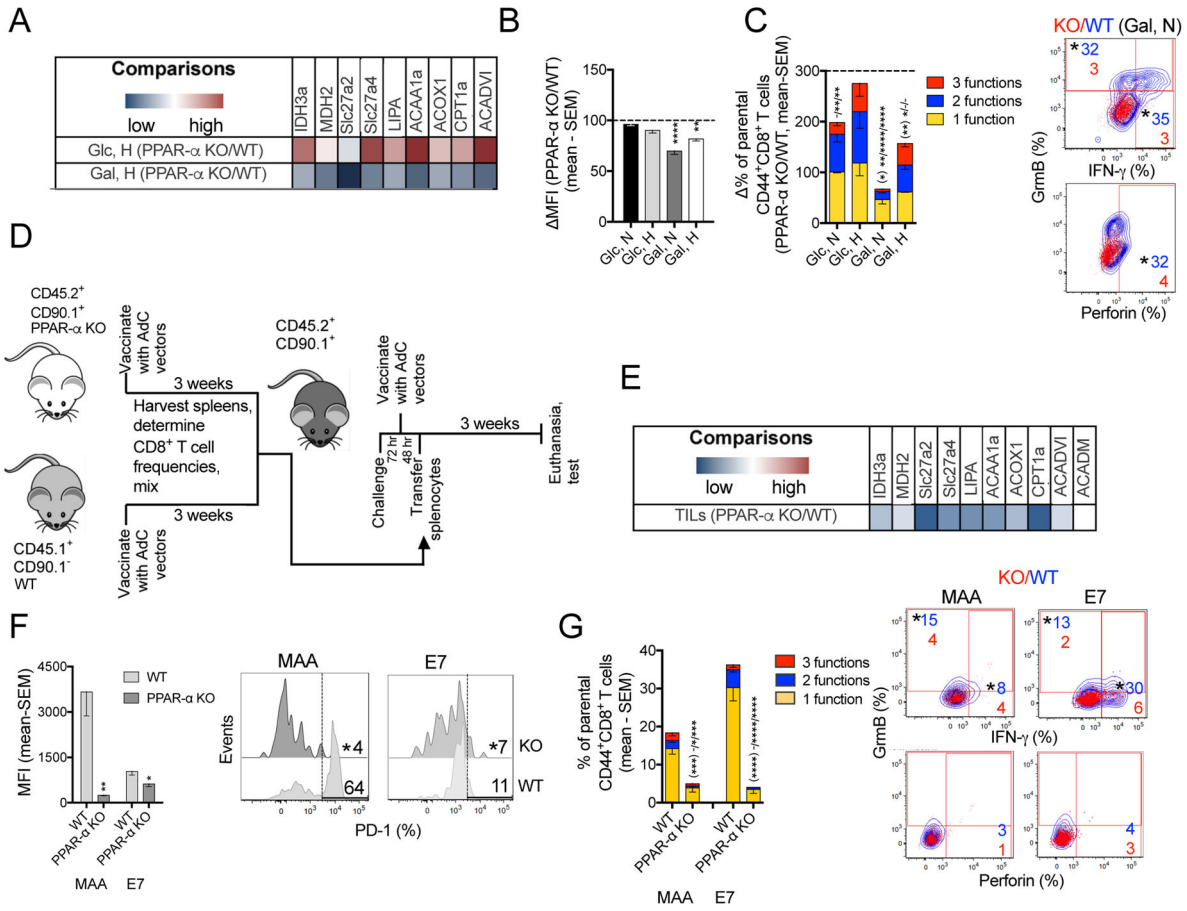

Figure 8. Inhibiting FA catabolism impairs CD8$^+$ T functions while decreasing PD-1 expression

(A) Transcript levels comparing CD8$^+$ T cells from PPAR-α KO and WT mice stimulated in Glc- or Gal-medium under hypoxia (n=4). (B) Normalized MFIs for PD-1 on PPAR-α KO vs. WT activated CD8$^+$ T cells cultured under different conditions (n=4–5). (C) Left: Normalized % PPAR-α KO vs. WT CD8$^+$ T cells producing 3, 2, or 1 of the 3 tested functions (n=5). Right: Overlays of WT (blue) vs. PPAR-α KO (red) CD8$^+$ T cells cultured in Gal-medium under normoxia. (D) Experimental design. (E) Comparison of transcript levels in CD44$^+$CD8$^+$ TILs from PPAR-α KO vs. WT donors (n=3 mice/group). (F) MFI of PD-1 on WT and PPAR-α KO donor CD8$^+$ TILs with histograms. (G) Left: % donor-derived specific CD8$^+$ TILs from the two groups producing 3, 2, or 1 of the 3 tested functions; Right: Overlays of factor-producing WT (blue) vs. PPAR-α (red) donor-derived TILs. (F, G) n=6/group. Data represent 2 assays, shown as mean - SEM. See also Figure S8.